

An introduction to reinforcement learning for neuroscience

Kristopher T. Jensen^{1,2}

¹ Sainsbury Wellcome Centre, University College London

² Computational and Biological Learning Lab, University of Cambridge

kris.torp.jensen@gmail.com

Abstract

Reinforcement learning has a rich history in neuroscience, from early work on dopamine as a reward prediction error signal for temporal difference learning (Schultz et al., 1997) to recent work suggesting that dopamine could implement a form of ‘distributional reinforcement learning’ popularized in deep learning (Dabney et al., 2020). Throughout this literature, there has been a tight link between theoretical advances in reinforcement learning and neuroscientific experiments and findings. As a result, the theories describing our experimental data have become increasingly complex and difficult to navigate. In this review, we cover the basic theory underlying classical work in reinforcement learning and build up to an introductory overview of methods used in modern deep reinforcement learning that have found applications in systems neuroscience. We start with an overview of the reinforcement learning problem and classical temporal difference algorithms, followed by a discussion of ‘model-free’ and ‘model-based’ reinforcement learning together with methods such as DYNA and successor representations that fall in between these two categories. Throughout these sections, we highlight the close parallels between the machine learning methods and related work in both experimental and theoretical neuroscience. We then provide an introduction to deep reinforcement learning with examples of how these methods have been used to model different learning phenomena in the systems neuroscience literature, such as meta-reinforcement learning (Wang et al., 2018) and distributional reinforcement learning (Dabney et al., 2020). Code that implements the methods discussed in this work and generates the figures is also provided.

1 Introduction

Humans and other animals learn from their experiences. Sometimes, this takes the form of explicit demonstration, as is often the case in our educational system. However, we often have to infer a good course of action on the basis of trial and error together with feedback received from the world around us – sometimes implicit and sometimes explicit. This is well illustrated by the classical case study of Pavlov’s dogs, who learned to associate a so-called ‘conditioned stimulus’ (CS; e.g. the ringing of a bell) with the availability of food shortly after. Following a brief period of learning, the dogs would start to salivate in response to the CS in advance of any food actually being served. This suggests that the dogs had learned to associate the CS with the availability of ‘reward’ in the form of food, and that they produced an appropriate physiological response to take advantage of this food availability. Importantly, this occurred without any explicit instruction or description of the sequence of events preceding food being served. Instead, the dogs learned from their actual experience with their environment and the presence of a salient, rewarding stimulus.

Such passive stimulus-response predictions are also called ‘Pavlovian learning’ and have been commonly used in neuroscience to study learning from external rewards (Niv, 2009). This forms a specific instantiation of the concept of ‘reinforcement learning’, which is a general term for settings where an agent has to learn on the basis of reward signals from the environment rather than explicit demonstration, as is the case in ‘supervised learning’. Importantly, the past decades have shown that principles of reinforcement learning can be used to explain not just behaviour, but also neural activity in biological circuits (Niv, 2009). An explicit neural basis of RL was initially demonstrated in foundational work by Schultz et al. (1997), which showed that the firing rates of dopaminergic neurons in the Ventral Tegmental Area (VTA) reflect the difference

between expected and actual ‘value’ when animals received a juice reward following a CS consisting of a lever-press in response to a small light turning on. This provided a potential neural substrate of the classical ‘temporal difference’ learning algorithm, which has since been expanded to a wealth of evidence for reinforcement learning in neural dynamics (Niv, 2009; Dabney et al., 2020). However, these classical algorithms are generally restricted to simple problem settings, while humans and other animals are capable of solving complex high-dimensional problems involving extended planning and complex motor control. The field of ‘deep reinforcement learning’ has recently emerged to tackle such problems in a machine learning setting, which has led to impressive results across a range of tasks (Mnih et al., 2013; Schrittwieser et al., 2020; Wurman et al., 2022; Vinyals et al., 2019). Intriguingly recent research has demonstrated that these deep RL algorithms also have parallels in both behaviour and neural dynamics (Botvinick et al., 2020; Wang et al., 2018; Dabney et al., 2020; Jensen et al., 2023), suggesting that the field of neuroscience can continue to learn from advances in reinforcement learning.

In this review, we provide an overview of the reinforcement learning problem and popular algorithms, with a particular focus on parallels and uses of these algorithms in neuroscience. This overview starts from classical tabular TD learning and Q-learning algorithms, which have guided neuroscientific research for decades. We then consider the important distinction between model-based and model-free reinforcement learning, as well as methods that fall somewhere in the gray area between these extremes, and discuss their neural correlates. Finally, we generalize the tabular methods to the non-linear function approximation setting and the resulting deep RL methods, which have revolutionized machine learning in recent years. We do this with a focus on methods that have had a strong influence on neuroscience to give the reader a better idea of the mathematical and computational background of recent neuroscientific findings. These include the ‘meta-reinforcement learning’ model of PFC by Wang et al. (2018) and the ‘distributional reinforcement learning’ model of VTA dopaminergic neurons by Dabney et al. (2020) in particular. We hope this introduction to RL for neuroscience will be useful both for those who are interested in the theory underlying reinforcement learning in neuroscience and for those who want an overview of how the neuroscientific literature builds on principles from reinforcement learning theory. Throughout the paper, the focus will be on an intuitive understanding of the relevant RL methods, and explicit derivations are included only where we consider them conducive to such understanding. We refer to Sutton and Barto (2018) for a more in-depth treatment of the underlying theory.

2 Problem setting

Here we provide a short introduction to the reinforcement learning problem in a discrete state and action space with a finite time horizon. For a more general treatment, we refer to Sutton and Barto (2018). In the discrete problem setting, the environment consists of states $s \in \mathcal{S}$, and the agent can take actions $a \in \mathcal{A}$. The environment is characterized by transition and reward probabilities $p(s_{t+1}, r_t | s_t, a_t)$, where r_t is the reward at time t . We will use $r(s_t, a_t)$ to denote either the reward when it depends deterministically on the state and action, or its expectation otherwise. We will further make the *Markov assumption* that the next state only depends on the current state and action, $p(s_{t+1}, r_t | s_t, a_t, s_{t-1}, a_{t-1}, \dots, s_0, a_0) = p(s_{t+1}, r_t | s_t, a_t)$.

We can now define a *trajectory* $\tau = \{s_t, a_t, r_t\}_{t=0}^T$, where

$$p(\tau) = p(s_0) \prod_{t=0}^T p(s_{t+1}, r_t | s_t, a_t) p(a_t | s_t). \quad (1)$$

$p(a_t | s_t)$ is the probability of taking action a_t in state s_t , which is usually controlled by the agent and denoted a *policy* $\pi(a_t | s_t)$ (Figure 1A). The objective of the agent is to maximize the expected total discounted reward

$$J(\pi) = \mathbb{E}_{\tau \sim p(\tau)} [R_\tau] = \mathbb{E}_{\tau \sim p(\tau)} \left[\sum_{t=0}^T \gamma^t r_t | \tau \right], \quad (2)$$

where $R_\tau := \sum_{t=0}^T \gamma^t r_t | \tau$ and we have written $J(\pi)$ since the policy uniquely specifies J in a stationary environment. In Equation 2, γ is a ‘discount factor’, which stipulates that we should care more about

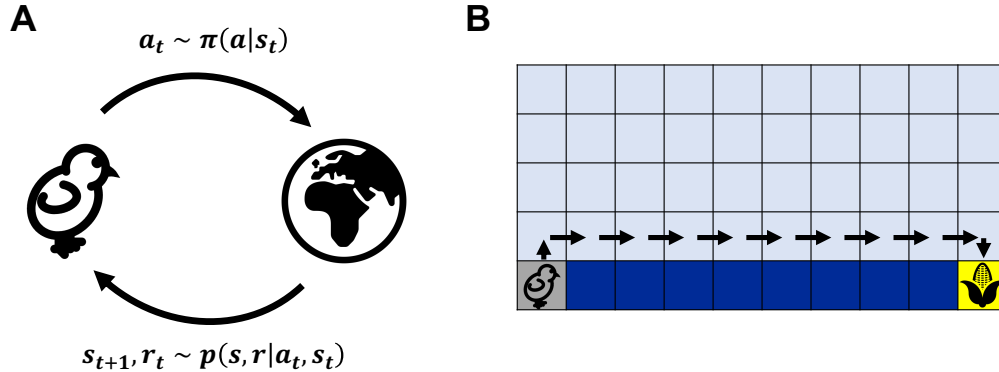


Figure 1: **The reinforcement learning problem and cliffworld environment.** (A) Illustration of the reinforcement learning problem. An agent (the chick) has to interact with the world to maximize its lifetime reward. This involves a balance between exploring potentially interesting states (e.g. learning to fly) while also exploiting states known to yield high reward (e.g. sitting in the nest and eating food brought back by its parents). At any given point in time, the chick is in some state s_t from which it can take an action a_t , with the probability of different actions determined by the ‘policy’ $\pi(a|s_t)$, which is controlled by the agent. a_t then leads to a change in the environment according to the non-controllable environment dynamics $s_{t+1}, a_t \sim p(s_{t+1}, r_t | s_t, a_t)$. Here, r_t is the empirical ‘reward’ received by the agent, and its objective is to collect as much cumulative reward as possible. Often, reinforcement learning problems are divided into ‘episodes’, with the agent learning over the course of multiple repeated exposures to the environment. This could for example consist of the chick learning over the course of multiple days when to wake up in anticipation of its parents bringing back food. (B) The ‘cliffworld’ environment, which will be used to demonstrate the performance and behaviour of a range of reinforcement learning algorithms in this work. The agent starts in the lower left corner (location $[0, 0]$), and the episode finishes when it encounters either the ‘cliff’ (dark blue) or the goal (yellow; location $[9,0]$). If the agent walks off the cliff, it receives a reward of -100. If it finds the goal, it receives a reward of +50. In any other state, it receives a reward of -1. Such negative rewards for ‘neutral’ actions are commonly used to encourage the agent to achieve its goal as fast as possible. The arrows indicate the ‘optimal’ policy, which takes the agent to the goal via the shortest possible route that avoids the cliffs.

immediate rewards than rewards far in the future. We can provide three interpretations for this discount factor. One is that agents intrinsically care more about immediate reward than distant reward. A second is that there is a finite probability $(1 - \gamma)$ of the current ‘episode’ or environment terminating or changing at each timestep, in which case we should weight putative future reward by the probability that we are still engaged in the task at that time. The third view is that γ simply provides a tool for reducing the variance of our learning methods, especially in temporally extended tasks. This third view is most compatible with the fact that *evaluation* of our RL agents at the end of training is generally done without any discounting.

Since $J(\pi)$ depends on the policy of the agent, it is possible to search in the space of policies for one that maximizes J , which is the topic of reinforcement learning. It is often assumed that the experience $\{\tau\}$ is generated by the agent acting according to its policy, and the resulting experience is then used to update the policy in a way that increases $J(\pi)$. However, ‘off-policy’ and ‘offline’ reinforcement learning methods also exist, where the agent learns on the basis of experience generated by a policy different from π (Levine et al., 2020; Section 9.3).

3 Temporal difference learning

In classical temporal difference learning, we want to learn a *value function* for a given state s and policy π , which specifies the expected future reward when following π starting from s :

$$V_\pi(s) = \mathbb{E}_{a \sim \pi} \left[\sum_{t' \geq t} \gamma^{t'-t} r_{t'} \mid s_t = s \right]. \quad (3)$$

Here, $\mathbb{E}_{a \sim \pi}[\cdot]$ indicates an expectation taken over trajectories τ resulting from the agent following the policy π . For the true value function, we can expand this as a self-consistency equation

$$V_\pi(s) = r(s) + \sum_{s'} p_\pi(s_{t+1} = s' \mid s_t = s) \mathbb{E}_{a \sim \pi} \left[\sum_{t'=t+1} \gamma^{t'-t} r_{t'} \mid s_{t+1} = s' \right] \quad (4)$$

$$= r(s) + \gamma \sum_{s'} p_\pi(s_{t+1} = s' \mid s_t = s) V_\pi(s'), \quad (5)$$

where $p_\pi(s_{t+1} = s' \mid s_t = s) = \sum_a \pi(a \mid s) p(s_{t+1} = s' \mid s_t = s, a_t = a)$ is the probability of transitioning from s to s' under π . Importantly, Equation 5 would not hold if $V_\pi(s)$ was not the true value function (Sutton and Barto, 2018). When learning an approximate value function $V(s_t)$, we can therefore use this bootstrapped self-consistency relation as an objective function:

$$\mathcal{L} \propto (V(s_t) - (r(s_t) + \gamma \mathbb{E}_\pi V(s_{t+1})))^2, \quad (6)$$

Gradient descent w.r.t $V(s_t)$ gives us an update rule

$$\Delta V(s_t) \propto -\frac{\partial \mathcal{L}}{\partial V(s_t)} \quad (7)$$

$$\propto -V(s_t) + r(s_t) + \gamma \mathbb{E}_\pi [V(s_{t+1})] \quad (8)$$

$$\approx -V(s_t) + r_t + \gamma V(s_{t+1}). \quad (9)$$

The last line approximates the expectation over next states with a single sample corresponding to the state and reward actually experienced. As more and more experience is collected and many small gradient steps are taken according Equation 9, these single-sample estimates will average out to the expectation in Equation 8 (Figure 2A). Variants of this algorithm can also learn about multiple past states at once using the notion of *eligibility traces* (Sutton and Barto, 2018). However, Equation 9 is the canonical temporal difference learning rule, and it leads to learning dynamics where the temporal difference error $\delta := -V(s_t) + r(s_t) + \gamma \mathbb{E}_\pi [V(s_{t+1})]$ is progressively propagated from the rewarding state to prior states that predict the upcoming reward. This forms the basis of the ‘temporal difference’ signal proposed to be represented in dopaminergic VTA neurons (Schultz et al., 1997). At the behavioural level, such theories of dopamine as a reinforcing signal are consistent with experiments showing that stimulation of dopamine neurons can be a strong driver of learning in instrumental conditioning tasks, where animals have to take explicit actions to achieve rewarding outcomes (Olds and Milner, 1954; Tsai et al., 2009). A wealth of other research also suggests a close correspondence between midbrain dopaminergic neural activity and temporal difference learning, and we refer to Niv (2009) and others for a more comprehensive overview.

In Equation 9, we simply learned a function for predicting reward without using this as the basis of taking good actions. Indeed, in classical Pavlovian conditioning, there are only states which happen in a predetermined order with no intervention or control on the part of the agent. However, having learned a value function, it is simple to use it for action selection if we can estimate $p(s_{t+1} \mid s_t, a_t)$. In this case, the expected reward associated with action a can be written as

$$\mathbb{E} \left[\sum_{t'=t} \gamma^{t'-t} r_{t'} \mid a_t = a \right] = r(a_t, s_t) + \gamma \sum_{s_{t+1}} p(s_{t+1} \mid s_t, a_t) V(s_{t+1}). \quad (10)$$

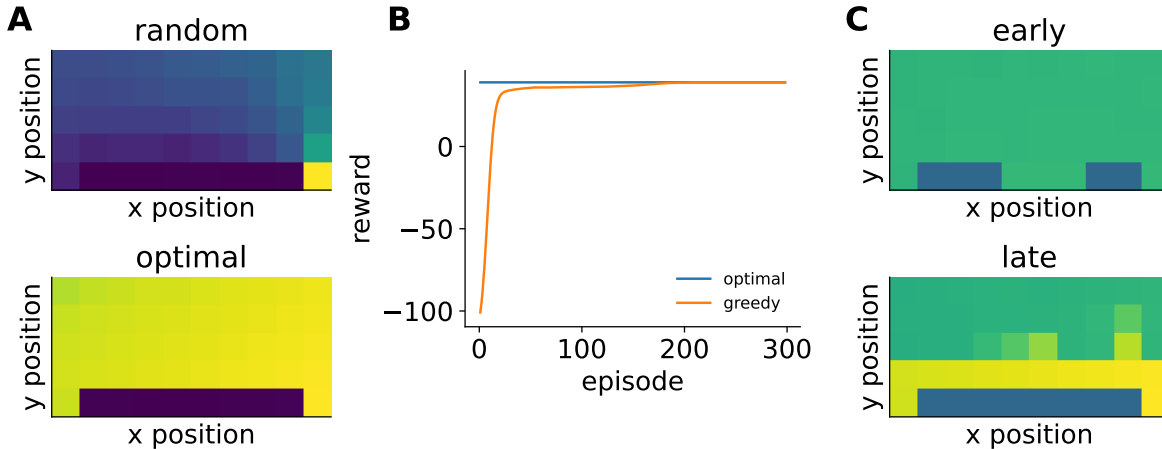


Figure 2: **Temporal difference learning.** (A) Value functions acquired through temporal difference learning (Equation 9) while acting according to either a random (top) or an optimal (bottom) policy. These simulations were performed with a random start state in the cliffworld environment to ensure full coverage of the space. Dark blue indicates negative expected reward (-100) and yellow indicates positive expected reward (+50). For these simulations, we used a learning rate of $\delta = 0.05$ and no temporal discounting ($\gamma = 1$). Under the random policy, states near the cliff have low value even though they are close to the goal, since the agent will often fall off the cliff from there. Under the optimal policy, all states have high expected reward, since the agent will always find the goal. States nearer the goal have higher value than those further away, although this is hard to distinguish on this color scale. (B) Empirical reward as a function of episode number for a TD-learning agent that acts according to Equation 11 while updating its value estimates according to Equation 9. For this agent, action selection assumes access to a ‘one-step’ world model in order to evaluate the consequence of each putative action. We see that the agent gradually converges to an optimal policy. Parameters for the agent are as in (A). (C) Value function learned by a greedy TD agent as in (B), plotted either early (top) or late (bottom) in training. Early in training, the agent has learned that the cliff is bad but doesn’t know where the goal is or how to get there. Late in training, the agent has learned a value function that locally resembles the optimal value function from (A), while it has not learned the value of distant states that are rarely or never visited. This is a potential shortcoming of ‘greedy’ agents that can easily converge to a sub-optimal local maximum in more complicated environments. For this analysis, we used a high learning rate of $\delta = 0.5$ to make the early TD updates larger and therefore more visible.

We can then perform action selection by choosing the action with the highest expected reward,

$$a^*(s) = \operatorname{argmax}_a \left(r(s, a) + \gamma \sum_{s_{t+1}} p(s_{t+1} | s_t, a_t) V(s_{t+1}) \right). \quad (11)$$

Updating the value function according to Equation 9 while acting in the environment according to Equation 11 leads to an agent that gradually learns to take better actions as it learns a better value function (Figure 2B-C).

4 Q-learning

An alternative approach for learning to select good actions (the so-called ‘control problem’) when we don’t know the transition structure of the world is to learn the value of taking action a in state s instead of only learning the value of the state. This gives rise to ‘Q-learning’ methods, where we learn the *state-action values*

$$Q_\pi(s, a) = \mathbb{E}_{a \sim \pi} \left[\sum_{t'=t} \gamma^{t'-t} r_{t'} | s_t = s, a_t = a \right]. \quad (12)$$

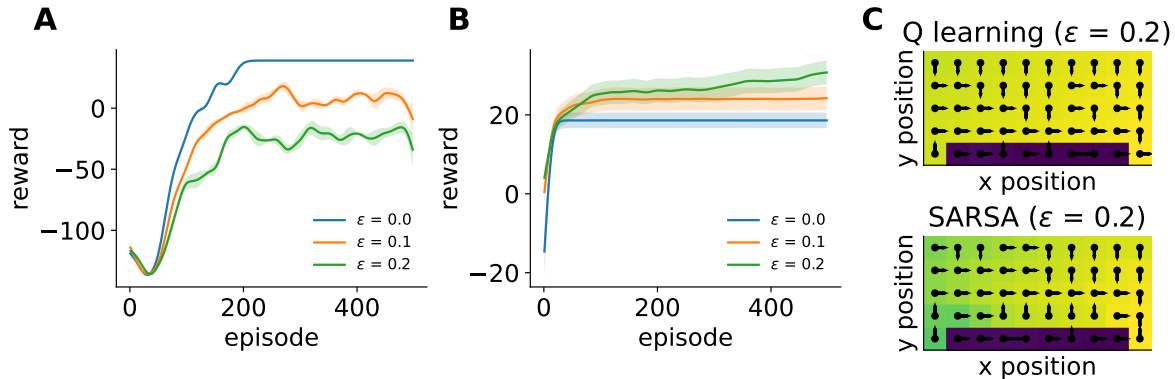


Figure 3: **Q-learning.** (A) Empirical reward as a function of episode number for Q-learners with different levels of stochasticity in their policy ($\epsilon \in \{0, 0.1, 0.2\}$; legend). For these simulations, we used a learning rate of $\delta = 0.05$ for all agents and no temporal discounting ($\gamma = 1$). The agent with $\epsilon = 0$ converges to an optimal policy, similar to the TD agent in Figure 2A. However, convergence is in this case slower despite using the same learning rate, because the Q-learner has to learn about each action independently, while the TD agent used its one-step world model to aggregate learning across actions reaching the same state. In this cliffworld environment, increasing epsilon leads to worse performance since it increases the probability of falling off the cliff. Additionally, there is no risk of getting stuck in a local minimum since there is only one rewarding state, which decreases the value of exploration. Lines and shading indicate mean and standard error across 10 simulations. (B) As in (A), now for a non-cliffworld grid environment with two goals: one with a reward of +20 at location (0, 4), and one with a reward of +50 at location (5,0). In this case, having non-zero epsilon can increase the probability of discovering the ‘high reward’ goal rather than getting stuck with a locally optimal policy of moving to the ‘low reward’ goal. In these simulations, we used a learning rate of $\delta = 1$, since this effect is less robust with lower learning rates that lead to more exploration of the environment across all agents. (C) Policy learned by a Q-learning (top) or a SARSA (bottom) agent with $\epsilon = 0.2$. Colours indicate the maximum value of any action in a state from blue (-100) to yellow (+50), and arrows indicate which action has the highest value. The Q-learning agent learns to move right above the cliff, because this is the optimal thing to do under the assumption that subsequent actions are also optimal. This is because it is an ‘off-policy’ algorithm that does not take into account the actual policy of the agent. In contrast, the SARSA agent learns to move a ‘safe distance’ away from the cliff, since it is an ‘on-policy’ algorithm that takes into account the finite probability of the agent choosing to move off the cliff from upcoming states. Q-learning agents are also frequently trained using a stochastic ϵ -greedy policy and then evaluated with the greedy policy corresponding to $\epsilon = 0$, or they can be trained while ‘annealing’ ϵ from some finite value to 0 over many episodes.

Given these state-action values, it is simple to perform action selection by taking the action with the highest expected reward in a given state,

$$a^*(s) = \operatorname{argmax}_a Q(s, a). \quad (13)$$

To learn the Q -values necessary for such action selection, we start by expanding Equation 12,

$$Q_\pi(s_t, a_t) = r(s_t, a_t) + \gamma \sum_{s_{t+1}} p(s_{t+1}|s_t, a_t) \sum_{a_{t+1}} \pi(a_{t+1}|s_{t+1}) Q_\pi(s_{t+1}, a_{t+1}). \quad (14)$$

For the greedy policy $\pi^g(a|s) := \delta(a, a^*(s))$, this gives rise to a self-consistency expression for the state-action values:

$$Q_{\pi^g}(s_t, a_t) = r(s_t, a_t) + \gamma \mathbb{E}_{s_{t+1} \sim p(s_{t+1}|s_t, a_t)} [\max_{a_{t+1}} Q_{\pi^g}(s_{t+1}, a_{t+1})]. \quad (15)$$

Importantly, this self-consistency expression only holds when the Q -values have converged to the true expected rewards, and the associated greedy policy is therefore optimal (Sutton and Barto, 2018). We can now use Equation 15 as a loss function by defining

$$\mathcal{L} \propto (Q(s_t, a_t) - (r(s_t, a_t) + \gamma \mathbb{E}_{s_{t+1} \sim p(s_{t+1}|s_t, a_t)} [\max_{a_{t+1}} Q(s_{t+1}, a_{t+1})]))^2, \quad (16)$$

Gradient descent w.r.t $Q(s_t, a_t)$ gives us an update rule

$$\Delta Q(s_t, a_t) \propto -\frac{\partial \mathcal{L}}{\partial Q(s_t, a_t)} \quad (17)$$

$$\propto -Q(s_t, a_t) + r(s_t, a_t) + \gamma \mathbb{E}_{s_{t+1} \sim p(s_{t+1}|s_t, a_t)} [\max_{a_{t+1}} Q(s_{t+1}, a_{t+1})] \quad (18)$$

$$\approx -Q(s_t, a_t) + r_t + \gamma \max_{a_{t+1}} Q(s_{t+1}, a_{t+1}). \quad (19)$$

This is the so-called Q-learning update rule (Watkins, 1989; Figure 3A), where we have again estimated the expectation over next states with the single sample actually seen by the agent.

Q-learning is guaranteed to converge to the optimal policy in the limit of infinitesimal learning rates and infinite sampling of the state-action space (Watkins and Dayan, 1992; Sutton and Barto, 2018). However, following the greedy policy $a^*(s) = \operatorname{argmax}_a Q(s, a)$ before convergence of the Q values can lead to undersampling of the state-action space and poor performance. It is therefore common to either use an ‘ ϵ -greedy’ policy, $\pi(a|s) = \epsilon/|\mathcal{A}| + (1-\epsilon)\delta(a, a^*(s))$, or a softmax-policy, $\pi(a|s) \propto \exp(\beta Q(a, s))$, to collect the experience used to update the Q values (Figure 3B). These approaches give rise to so-called ‘off-policy’ algorithms, since the policy used in the learning update (the greedy policy) is different from the policy used for action selection (the stochastic policy). An on-policy version of Q-learning known as ‘SARSA’ (state-action-reward-state-action) is also commonly used, where the Q-learning update uses the Q-value corresponding to the action a_{t+1} sampled at the next timestep instead of the greedy action (Figure 3C):

$$\Delta Q(s_t, a_t) \propto -Q(s_t, a_t) + r_t + \gamma Q(s_{t+1}, a_{t+1}). \quad (20)$$

This will converge to the true Q values for a given policy π , similar to how the TD learning rule in Equation 9 is guaranteed to converge to the true value function for a given policy, again under assumptions of infinite sampling of the space. In ‘instrumental conditioning’ settings, where animals have to choose between multiple actions with different values, studies have also found evidence for midbrain dopamine neurons encoding either quantities resembling the prediction error used for Q learning (Roesch et al., 2007; Niv, 2009) or SARSA (Morris et al., 2006; Niv, 2009).

5 Model-free and model-based reinforcement learning

In the previous section, we developed a so-called ‘model-free’ reinforcement learning algorithm. This involves learning a stimulus-response pattern that says ‘when in state s , take action a ’. Such algorithms do not require much computation at decision time, where there is no need to plan far into the future. However, it can require a lot of experience with the environment to learn these model-free policies, and they can be very inflexible in changing environments.

On the other hand, ‘model-based’ reinforcement learning uses a model of the world to simulate the consequences of different actions at decision time. This can be much more data efficient, since learning a world model is often simpler than learning a full policy (Figure 4A). However, model-based decision making can also be computationally intensive at decision-time in complicated state spaces (Figure 4B). Such models have recently exhibited impressive performance across a range of RL settings with large state spaces, including atari, chess, shogi, and Go (Silver et al., 2018; Schrittwieser et al., 2020; Deisenroth and Rasmussen, 2011).

In model-based RL, experience is used to learn a transition-and-reward function $p(s_{t+1}, r_t | s_t, a_t)$ from past experience. Once this model has been learned, it can be used for planning at decision time. This can be done for example by expanding the Q-value relation from Equation 15:

$$Q(s_t, a_t) = r_t + \gamma \mathbb{E}_{p(s_{t+1}|s_t, a_t)} \left[\operatorname{argmax}_{a_{t+1}} Q(s_{t+1}, a_{t+1}) \right] \quad (21)$$

$$= r_t + \gamma \mathbb{E}_{p(s_{t+1}|s_t, a_t)} \left[\operatorname{argmax}_{a_{t+1}} \left[r(a_{t+1}, s_{t+1}) + \gamma \mathbb{E}_{p(s_{t+2}|s_{t+1}, a_{t+1})} \left[\operatorname{argmax}_{a_{t+2}} Q(s_{t+2}, a_{t+2}) \right] \right] \right] \quad (22)$$

$$= \dots \quad (23)$$

If the environment is deterministic, $p(s_{t+1}|s_t, a_t)$ is a delta function, and otherwise the next-state expectations may need to be approximated with multiple samples. Unfortunately, the optimization over all possible action

sequences in Equation 21 is in general an exponentially large search problem in the planning depth, which makes it infeasible for any reasonably sized problem setting. It is therefore common to either use ‘depth-first search’ with limited breadth, or ‘breadth-first search’ with limited depth. In breadth-first search, we consider all possible actions at each level of the search tree but terminate the search at a finite depth, instead using cached ‘model-free’ state-values to estimate the reward-to-go from the termination of the search. This kind of ‘plan-until-habit’ algorithm has also been proposed as a model of human behaviour (Keramati et al., 2016). In depth-first search, we instead sample a series of paths from s_t all the way to termination (or some upper bound), using a heuristic to prioritize actions expected to be good, and then pick a path associated with high expected reward. This is what is implemented in most Monte Carlo tree search (MCTS) methods, such as AlphaZero (Silver et al., 2018), which uses a hardcoded transition function, and MuZero (Schrittwieser et al., 2020), which uses a learned transition function. In both of these approaches, neural networks are used (i) to estimate the ‘reward-to-go’ if the maximum search depth is reached before termination, and (ii) to select which actions to evaluate during the search process. Methods for learning such value functions and policies in neural networks are covered in more detail in Section 7.

A shortcoming of these MCTS-based approaches from a neuroscientific perspective is that they often perform a large number of node expansions at each decision point. For example, MuZero and AlphaZero perform 800 rollouts to a leaf node for each decision that they make. While this can be done very quickly on a computer, it seems unrealistic as a model of human decision making. In some settings, it is possible to use more efficient algorithms once a model has been learned, such as Dijkstra’s algorithm or A^* -search in shortest-path problems (Hart et al., 1968). However, it is in general necessary to somehow trade off the temporal opportunity cost of planning with the improvement in policy and expected reward (Botvinick and Cohen, 2014; Agrawal et al., 2022). This has been a popular research area in cognitive science, where a wealth of literature on ‘resource-rational’ decision making has emerged in recent years (Griffiths et al., 2019; Callaway et al., 2022). However, this literature has often considered optimal behaviour in simple tasks with less focus on the learning process and neural mechanisms that might implement the necessary computations. Bridging this gap, recent work has suggested that frontal cortex might initially store a ‘model-free’ policy in its network state and gradually update this with model-based information from the hippocampal formation in cases where the policy improvement is expected to make up for the temporal opportunity cost (Jensen et al., 2023). In this work, the authors found substantial policy improvements from only a few rollouts (Vul et al., 2014), and the ‘reaction times’ of the agent exhibited similar task-related structure to human behaviour.

While several model-based and model-free reinforcement learning methods have thus been developed and used to model animal learning and behaviour, it remains an open question when and whether different approaches are used. A different line of research has explicitly investigated the trade-offs between model-based and model-free RL in biological agents (Daw et al., 2005; Geerts et al., 2020; Lengyel and Dayan, 2007), where the choice between the two approaches is thought to be guided by some notion of optimality on the basis of available resources and uncertainty about the environment. A popular paradigm for such studies attempting to distinguish between model-free and model-based behaviour is the so-called ‘two-step’ task developed by Daw and colleagues (Daw et al., 2011; Momennejad et al., 2017; Wang et al., 2018; although note Akam et al., 2015).

It has generally been accepted that humans can use both model-free and model-based decision making, with the dorsolateral striatum being particularly important for model-free reinforcement learning (Yin et al., 2004, 2005), and the dorsomedial striatum, prefrontal cortex, and hippocampal formation being important for model-based decision making (Vikbladh et al., 2019; Geerts et al., 2020; Miller et al., 2017; Niv, 2009; Killcross and Coutureau, 2003). This has interesting parallels to recent work in the motor learning literature, where the basal ganglia were found to be sufficient for ‘habitual’ motor sequences even in the absence of motor cortex, while motor cortex was necessary for more flexible motor behaviours that are likely to require a high-level ‘schema’ of the task structure (Mizes et al., 2023b,a).

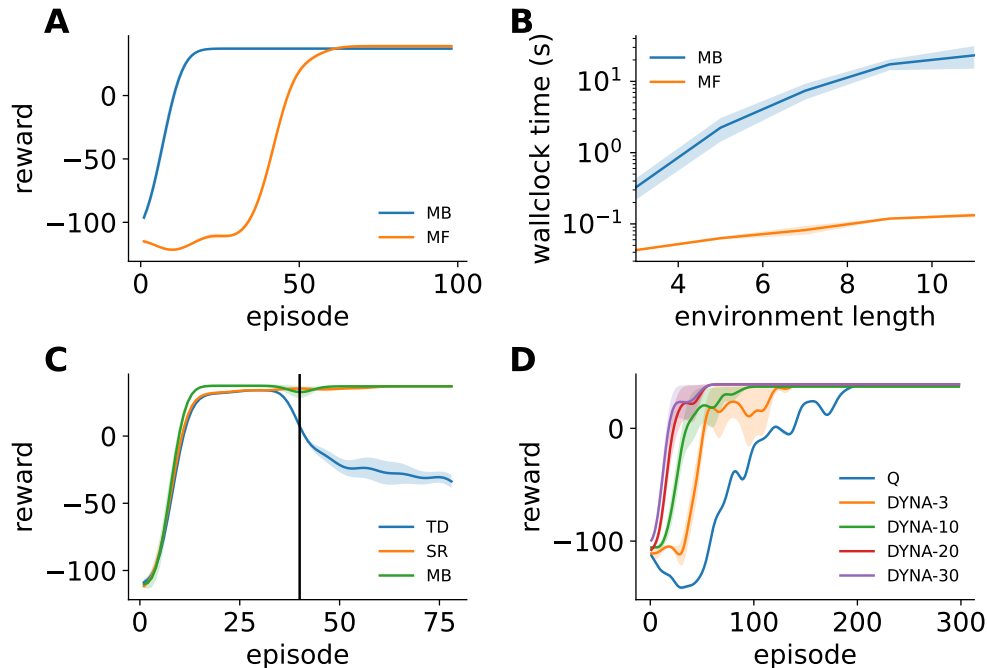


Figure 4: **Model-based reinforcement learning.** (A) Learning curves for model-based (MB) and model-free (MF) RL agents. In this case, the MB agent used a depth-first search to compute an optimal path at each decision point. If a shorter path to a given state had already been discovered, the search was not continued. The reward and transition functions of the agent were initialized to zero and the empty set respectively, and they were gradually populated as the agent explored the environment across episodes. The MF agent was a simple Q-learning agent with $\epsilon = 0$ and $\delta = 1$. The MB agent requires substantially less experience than the MF agent for a given level of performance. (B) Wallclock time needed to run 100 episodes of cliffworld with either the MB or MF agents from (A), as a function of the length of the environment. Although (A) shows that the MB agent requires substantially less experience to learn a good policy, the wallclock time per episode was much larger than that required by the MF agent. This illustrates an important balance between model-based and model-free reinforcement learning, where MF methods usually require more experience but MB methods require more compute for a given level of experience. In domains such as robotics, where collecting data is very time consuming, MB methods can still be a more efficient way to reach a high level of performance. (C) Learning curve for an agent using the successor representation (SR) together with learning curves for the model-based agent in (A) and the greedy TD-agent from Figure 2. At episode 40 (vertical black line), the goal was moved from location (9, 0) to location (0, 4), and location (9, 0) was instead given a reward of -5. The MB and SR agents had their reward functions updated to reflect this change and were immediately able to adapt their policies, while the TD agent had no such mechanism for robustness to changing reward functions. It is worth noting that an SR agent cannot always adapt to a new reward function if the newly rewarded states have low probability under the old policy, since the successor matrix itself is a function of the policy. Reward curves were convolved with a Gaussian kernel ($\sigma = 3$ episodes), which is why performance appears to decrease slightly before episode 40 for the TD agent. In this simulation, the TD and SR agents were assumed to have access to a 1-step world model at initialization, while the MB agent had to learn the transition structure from experience. This is why the MB agent does not exhibit faster initial learning than the SR and TD agents. (D) Learning curve for a standard Q-learning agent (blue) or DYNA agents that perform different numbers of Q value updates for each step of physical action (legend). In this case, the DYNA updates simply used cached experience rather than data from a learned world model. We see that DYNA agents are able to make better use of limited experience, although this comes at the cost of increased compute (proportional to the number of updates).

6 The successor representation

As we saw in the previous section, an important distinction can be made between model-free reinforcement learning methods, which cache stimulus-response mappings based on prior experience, and model-based reinforcement learning methods, which compute a policy by simulating possible futures using a world model at decision-time. However, [Dayan \(1993\)](#) introduced a new formulation of the reinforcement learning reward function known as the ‘successor representation’ (SR), which combines some of the features of model-free and model-based reinforcement learning. In particular, the SR allows for flexible adaptation to changing reward functions without having to perform expensive simulations at decision time.

This formulation rewrites the expected reward starting from state s as

$$V_\pi(s) = \mathbb{E}_\pi \left[\sum_{t=0}^{\infty} \gamma^t r_t | s_0 = s \right] \quad (24)$$

$$= \sum_{t=0}^{\infty} \gamma^t \sum_{s'} p_\pi(s_t = s' | s_0 = s) r(s') \quad (25)$$

$$= \sum_{s'} r(s') \sum_t \gamma^t p_\pi(s_t = s' | s_0 = s) \quad (26)$$

$$= \mathbf{r}^T \mathbf{m}_s^\pi. \quad (27)$$

Here, \mathbf{r} is a vector of the reward associated with each state, and \mathbf{m}_s^π is a vector of the expected discounted future occupancy of state s' given that the agent starts in state s and follows the policy π :

$$M_{ss'}^\pi = \sum_{t=0}^{\infty} \gamma^t p_\pi(s_t = s' | s_0 = s). \quad (28)$$

The full matrix \mathbf{M}^π , constructed from stacking the \mathbf{m}_s^π corresponding to all states s , is denoted the ‘successor matrix’, and constructing it allows us to write down a vector of expected rewards from any state s as

$$\mathbf{v}_\pi = \mathbf{M}^\pi \mathbf{r}. \quad (29)$$

Here, we have retained the superscript π to indicate that the successor matrix depends on the policy of the agent, which affects the expected occupancy of different states. Since this allows us to compute the value of each state, we can perform action selection using [Equation 11](#).

The flexibility of the successor representation arises when the reward structure of the environment changes, $\mathbf{r} \rightarrow \mathbf{r}'$. We can now compute the expected reward associated with each state under the new reward function and old policy,

$$\mathbf{v}'_\pi = \mathbf{M}^\pi \mathbf{r}'. \quad (30)$$

Of course this new value function will lead to us eventually changing our policy and having to update \mathbf{M} , but it provides a better starting point than using the wrong policy *and* value function as in standard temporal-difference learning ([Figure 4C](#)). Additionally, it has the appealing feature that the successor matrix can be learned by simple temporal-difference learning when transitioning from s_t , analogous to [Equation 9](#):

$$\Delta M_{s_t s'} \propto -M_{s_t s'} + \delta(s_t, s') + \gamma M_{s_{t+1} s'}. \quad (31)$$

Here, s' is the set of all other states, s_{t+1} is the next state actually observed, and the learning rule says that transitioning from s_t to s_{t+1} means that (i) we have just been in state s_t , and (ii) we should increase the expected occupancy of all states commonly reached from s_{t+1} (including s_{t+1} itself). Alternatively, if the transition matrix \mathbf{T} is known, where $T_{ss'} = p_\pi(s_{t+1} = s' | s_t = s)$, the successor matrix can be computed as the geometric series $\mathbf{M} = \mathbf{I} + \gamma \mathbf{T} + \gamma^2 \mathbf{T}^2 + \dots = (\mathbf{I} - \gamma \mathbf{T})^{-1}$.

The SR has also been proposed as a model of how humans and other animals learn and generalize ([Momennejad et al., 2017](#); [Stachenfeld et al., 2017](#); [Geerts et al., 2020](#); [Gershman, 2018](#)). For example, humans have been shown to be able to adapt more readily to changes in the reward function than changes in the transition

function in a simple sequential binary decision-making task (Momennejad et al., 2017), consistent with the SR facilitating rapid adaptation to changes in \mathbf{r} but only slow learning of \mathbf{M} . Additionally, hippocampal ‘place cells’ have been proposed to encode a predictive map, with each cell corresponding to a column of \mathbf{M} (Stachenfeld et al., 2017). In this model, the firing of a place cell in a given location s reflects the expected future occupancy of its ‘preferred’ location s' conditioned on currently being at s . Stachenfeld et al. (2017) showed that the SR model explains a range of findings in the hippocampal literature, including asymmetric place fields on a one-dimensional track (Mehta et al., 2000) and local remapping of place fields near a barrier (Alvernhe et al., 2011).

While the SR is perhaps the most prominent model in systems neuroscience that combines features of model-free and model-based RL, it is not the only one. Another interesting approach that has found parallels in the neuroscience literature is the ‘DYNA’ architecture of Sutton (1991). In this framework, a model of the world is learned from experience and used to train a model-free policy offline by bootstrapping imagined experience sampled from the model. This allows for more data-efficient learning of model-free policies at the cost of additional compute during ‘rest’ but without necessarily needing more compute at decision time, in contrast to the model-based approaches discussed previously (Figure 4D). The model used to simulate data for offline training can either be an explicit learned world model, or it can simply be a memory buffer of past experiences in the form of $(s_t, a_t, r_t, s_{t+1}, a_{t+1})$ tuples. Such experience replay has proven crucial to the success of modern deep reinforcement learning agents by allowing for higher data efficiency and reducing the instability arising from the autocorrelated nature of online experience (Mnih et al., 2013; Schaul et al., 2015). A prominent theory in neuroscience suggests that hippocampal replays could be implementing such a DYNA-like algorithm by generating imagined experience used to train the model-free RL systems of the brain (Mattar and Daw, 2018). This theory is supported by the finding that the patterns of replay exhibited by rodents in various navigation tasks are consistent with the optimal replays of a Q-learning agent with DYNA.

7 Deep reinforcement learning

So far, we have considered the setting of small state- and action-spaces, for which we can simply learn a tabular policy. However, in many realistic settings, the state space is large enough that we cannot enumerate all possible states and actions. In these cases, we instead have to rely on *function approximation* (Sutton and Barto, 2018). This approach makes the assumption that similar states will also be associated with similar state-action value functions and should therefore have similar policies. By making this assumption, we can generalize to unseen states based on our previous experience, provided that our function approximator is sufficiently good. Recent years have seen incredible progress in this setting by using deep or recurrent neural networks as powerful function approximators for reinforcement learning – the domain of ‘deep reinforcement learning’. This approach has seen an increase in interest not just in the machine learning literature, but recently also as a model of neural dynamics and behaviour in humans and other animals (Wang et al., 2018; Jensen et al., 2023; Makino, 2023; Merel et al., 2019; Banino et al., 2018). For a more comprehensive overview of the links between deep RL and neuroscience, we refer the interested reader to Botvinick et al. (2020). Modern approaches in (model-free) deep RL can largely be divided into two categories: policy gradient methods and deep Q learning. In policy gradient methods, we directly train the network to output a policy, whereas deep Q networks (DQNs) output a set of state-action values that can be used for action selection.

Policy gradient methods

The conceptually simplest approach for deep reinforcement learning relies on the so-called policy gradient methods (Sutton and Barto, 2018). In this approach, we train a neural network with parameters θ to take as input the (observable) state of the environment and directly output a policy π_θ . Our goal is then to find the setting of θ that maximizes the expected reward in Equation 2. A conceptually simple way to achieve

this would be to define $R_\tau := \sum_{t=0}^T \gamma^t r_t$ and use gradient descent with gradients given by

$$\nabla_\theta J(\theta) = \nabla_\theta \mathbb{E}_{\tau \sim \pi_\theta} [R_\tau] \quad (32)$$

$$= \sum_{\tau} R_\tau \nabla_\theta p_\theta(\tau). \quad (33)$$

Here, $\tau \sim \pi_\theta$ indicates trajectories sampled from the distribution over trajectories induced by policy π_θ , and $J(\theta)$ indicates the expectation of R_τ under π_θ (c.f. Equation 2). However, evaluating Equation 33 requires us to know how the environment will respond to our actions in order to compute the necessary derivatives, which in general may not be the case (although some model-based deep RL approaches train a differentiable predictive model of the environment to do this; Clavera et al., 2020). Instead, we use the ‘log-derivative trick’, which takes advantage of the linearity of the expectation and the identity $\nabla_\theta \log f(\theta) = f(\theta)^{-1} \nabla_\theta f(\theta)$ to write

$$\nabla_\theta J(\theta) = \sum_{\tau} R_\tau \nabla_\theta p_\theta(\tau) \quad (34)$$

$$= \sum_{\tau} R_\tau p_\theta(\tau) \nabla_\theta \log p_\theta(\tau) \quad (35)$$

$$= \mathbb{E}_{\tau \sim \pi_\theta} [R_\tau \nabla_\theta \log p_\theta(\tau)], \quad (36)$$

Since the environment does not depend on θ , we can simplify the calculation of $\nabla_\theta \log p_\theta(\tau)$:

$$\nabla_\theta \log p_\theta(\tau) = \nabla_\theta \left[\log p(s_0) + \sum_{t=0}^T \log p(s_{t+1} | s_t, a_t) + \log \pi_\theta(a_t | s_t) \right] \quad (37)$$

$$= \sum_{t=0}^T \nabla_\theta \log \pi_\theta(a_t | s_t). \quad (38)$$

Inserting Equation 37 in Equation 34 and taking a Monte Carlo estimate of the expectation, we arrive at the REINFORCE algorithm (Williams, 1992):

$$\nabla_\theta J(\theta) = \mathbb{E}_{\tau \sim \pi_\theta} \left[R_\tau \sum_{t=0}^T \nabla_\theta \log \pi_\theta(a_t | s_t) \right] \quad (39)$$

$$\approx \frac{1}{N} \sum_{\tau \sim \pi_\theta} \left(\sum_{t=0}^T \gamma^t r_t \right) \left(\sum_{t=0}^T \nabla_\theta \log \pi_\theta(a_t | s_t) \right). \quad (40)$$

Intuitively, Equation 40 says that we should preferentially upregulate the probability of trajectories with high reward, which will lead to downregulation of trajectories with lower reward due to the normalization of the policy. Importantly, Equation 40 no longer requires us to differentiate through the environment – only the policy.

While the REINFORCE algorithm is unbiased, it also has high variance, which can make learning slow and unstable. It is therefore common to introduce modifications, which can help reduce the variance. The first of these comes from noting that an action taken at time t cannot affect the reward received at times $t' < t$. This allows us to define $R_t := \sum_{t'=t}^T \gamma^{t'-t} r_{t'}$ and rewrite our REINFORCE update as

$$\nabla_\theta J(\theta) \approx \frac{1}{N} \sum_{\tau \sim \pi_\theta} \sum_{t=0}^T R_t \nabla_\theta \log \pi_\theta(a_t | s_t). \quad (41)$$

This is the formulation most commonly used, but it is worth noting that it is actually *not* the same as Equation 40, which would require us to use $R_t = \sum_{t'=t}^T \gamma^{t'-0} r_{t'}$. As briefly discussed in Section 2, this is because the discount factor γ is generally used as a variance reduction method rather than an indication that we intrinsically care less about rewards later in the task, although Equation 41 is also consistent with an interpretation of $(1 - \gamma)$ as a termination probability.

It is also straightforward to show that for a baseline $B(s_t)$ that does not depend on a_t ,

$$\mathbb{E}_{s_t, a_t \sim p_\theta(s_t, a_t)} [B(s_t) \nabla_\theta \log \pi_\theta(a_t | s_t)] = \int_{s_t} B(s_t) p(s_t) \left[\nabla_\theta \int_{a_t} \pi_\theta(a_t | s_t) da_t \right] ds_t \quad (42)$$

$$= \int_{s_t} B(s_t) p(s_t) [\nabla_\theta 1] ds_t = 0. \quad (43)$$

A corollary of this result is that we can subtract such a baseline from our empirical reward and still have an unbiased estimator while potentially reducing its variance. A common choice here is the expected future reward

$$V(s_t) = \mathbb{E} \left[\sum_{t'=t}^T \gamma^{t'-t} r_{t'} | s_t \right] \quad (44)$$

This gives rise to the so-called ‘actor-critic’ algorithm

$$\nabla_\theta J(\theta) \approx \frac{1}{N} \sum_{\tau \sim \pi_\theta} \sum_{t=0}^T (R_t - V(s_t)) \nabla_\theta \log \pi_\theta(a_t | s_t). \quad (45)$$

Intuitively, Equation 45 says that we should upregulate the probability of actions that lead to higher-than-expected reward and downregulate the probability of actions that lead to lower-than-expected reward. Interestingly, many studies in the neuroscience literature have suggested that the brain could be using something akin to an actor-critic algorithm, with dorsal striatum implementing the ‘actor’ and ventral striatum the ‘critic’ (Takahashi et al., 2008; Sutton and Barto, 2018).

Finally, it is common to reduce the variance of our gradient estimator through an approach known as ‘bootstrapping’. To implement this, we note that

$$\mathbb{E}[R_t] = \mathbb{E}[r_t + \gamma V(s_{t+1})]. \quad (46)$$

This is useful because $r_t + \gamma V(s_{t+1})$ has lower variance than R_t , so using this bootstrapped estimate of the reward-to-go can reduce the noise in our gradient estimate when using finite sample sizes. We therefore use $r_t + \gamma V(s_{t+1})$ to define the ‘advantage function’ $A_t = r_t + \gamma V(s_{t+1}) - V(s_t)$, which gives rise to the ‘advantage actor-critic’ (A2C) algorithm:

$$\nabla_\theta J(\theta) \approx \frac{1}{N} \sum_{\tau \sim \pi_\theta} \sum_{t=0}^T (r_t + \gamma V(s_{t+1}) - V(s_t)) \nabla_\theta \log \pi_\theta(a_t | s_t). \quad (47)$$

While we have considered two extreme cases of a full Monte Carlo estimate of R_t and a ‘one-step’ bootstrap, the sum in R_t can be truncated to any order with $R_{t'}$ replaced by $V(s_{t'})$. In theory, this estimator remains unbiased if our value function is correct. However, in practice the estimate of $V(s_{t'})$ learned by our critic will be inexact, which introduces a bias to our parameter updates. The bootstrapping procedure outlined above thus leads to a tradeoff between the bias and variance of our parameter updates, and the optimal tradeoff will depend on the problem setting, network architecture, and training paradigm being used.

For these actor-critic algorithms, it is common to parameterize both the policy $\pi_\theta(a_t | s_t)$ and the value function $V_\phi(s_t)$ with neural networks – often with a subset of shared parameters between θ and ϕ . This leaves the problem of updating the parameters. In order to use out-of-the-box automatic differentiation software, we do this by defining an auxiliary utility (i.e. negative loss)

$$\tilde{J}(\theta) = \frac{1}{N} \sum_{\tau \sim \pi_\theta} \sum_{t=0}^T (R_t - V(s_t)) \log \pi_\theta(a_t | s_t), \quad (48)$$

where R_t and $V(s_t)$ are treated as constant w.r.t. θ . In Equation 48 and the following equations, we can use either the empirical reward-to-go $R_t = \sum_{t' \geq t} \gamma^{t'-t} r_{t'}$, or we can use the bootstrapped estimate $R_t \approx r_t + \gamma V(s_{t+1})$. While $\tilde{J}(\theta)$ has no intrinsic interpretation, it is chosen such that

$$\nabla_\theta \tilde{J}(\theta) = \nabla_\theta J(\theta). \quad (49)$$

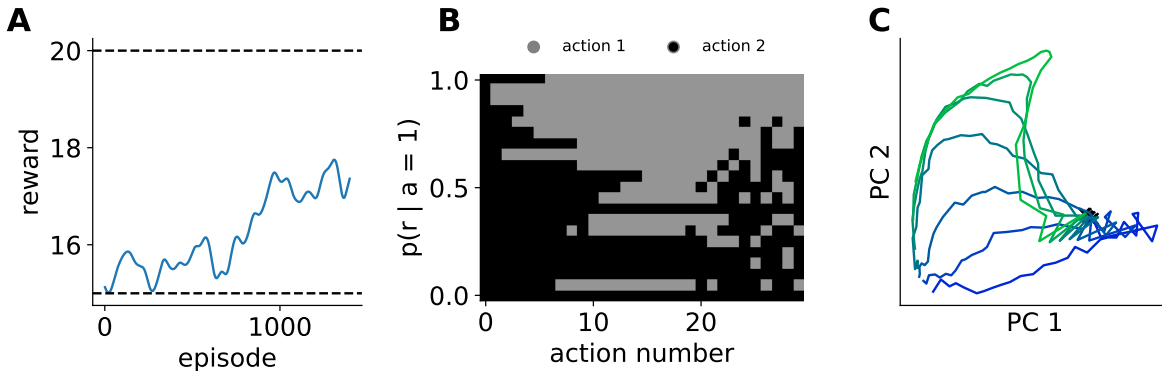


Figure 5: **Meta reinforcement learning.** The results in this figure reproduce some of the preliminary analyses in Figure 1 of Wang et al. (2018). (A) We trained a recurrent meta-reinforcement learning agent in a two-armed bandit task, where the reward probabilities of each arm were sampled independently from $\mathcal{U}(0, 1)$ at the beginning of each episode and remained fixed throughout the episode. A recurrent neural network was trained across many episodes with *different reward probabilities* using an actor-critic algorithm. The input to the agent consisted of the previous action, the previous reward, and the time-within-trial. The average reward per episode is plotted against the episode number, showing that the agent gradually learns to adapt within each episode to the particular instantiation of the bandit task. Importantly, the parameters of the network are fixed within an episode, meaning that this adaptation occurs through the recurrent dynamics. Dashed horizontal lines indicate the reward of an agent selecting random actions and an ‘oracle’ agent that always chooses the best arm. (B) Heatmap showing example behaviour of the agent in episodes with different reward probabilities for the first arm, $p(r|a = 1)$. For these plots, the probability of reward from the second arm was set to $p(r|a = 2) = 1 - p(r|a = 1)$. Across episodes, the agent experiments with different actions and eventually converges on taking the optimal action. For episodes with more symmetric reward probabilities (near the middle), it takes longer for the agent to identify the optimal action. This balance between exploration and exploitation is mediated by the recurrent network dynamics, which are learned over many episodes using deep reinforcement learning. (C) We averaged the hidden state of the RNN over 100 episodes for different reward probabilities, ranging from high reward for action 1 (blue) to low reward for action 1 (green), and performed PCA on the resulting matrix of average hidden states for different reward probabilities. This figure shows the 2-dimensional embedding of neural activity in the meta-RL agent, where we see that the agent converges to different regions of state space for different reward probabilities. Crosses indicate the hidden state at the beginning of each episode.

The gradient of the value function loss (i.e. negative utility) is given by

$$\nabla_{\phi} \mathcal{L}_V = \nabla_{\phi} \sum_t \frac{1}{2} (R_t - V_{\phi}(s_t))^2 = \sum_t -(R_t - V_{\phi}(s_t)) \nabla_{\phi} V_{\phi}(s_t). \quad (50)$$

When π_{θ} and V_{ϕ} share parameters, we also need to balance the gradients w.r.t. θ and ϕ in our update step. We do this by defining $\delta_t := R_t - V(s_t)$ (or $\delta_t := r_t + \gamma V(s_{t+1}) - V(s_t)$), introducing a hyperparameter β_V , and maximizing the joint utility

$$\mathcal{L} = \frac{1}{N} \sum_{\tau \sim \pi_{\theta}} \sum_{t=0}^T (\log \pi_{\theta}(a_t | s_t) + \beta_V V_{\phi}(s_t)) \delta_t. \quad (51)$$

Importantly, we do not propagate gradients w.r.t. ϕ or θ through the computation of δ_t . Finally, it is also common to add an auxiliary entropy loss of the form $\mathcal{L}_E = \beta_E \frac{1}{N} \sum_{\tau \sim \pi_{\theta}} \sum_{t=0}^T \sum_a \pi_{\theta}(a_t | s_t) \log \pi_{\theta}(a_t | s_t)$ to encourage exploration.

While these policy gradient methods may seem far removed from neuroscience, they have had several applications in the field in recent years. For example, Li et al. (2022) recently demonstrated that an off-policy variant known as the ‘soft actor-critic’ algorithm (Haarnoja et al., 2018) can be used to train an agent that shapes the behaviour of *C. elegans* via an optogenetic action space. Networks trained with policy gradient

algorithms have also recently attracted significant interest as models of learning and neural dynamics in the biological brain (Wang et al., 2018; Jensen et al., 2023; Merel et al., 2019). Of particular interest, Wang et al. (2018) suggested that frontal cortex can be well described as a *recurrent* deep RL agent, where the RNN parameters are configured by learning from rewards over long periods of time from many tasks that have a shared underlying structure. Importantly, this ‘slow’ model-free learning process gives rise to an agent that can rapidly learn from experience with *fixed parameters* when exposed to a new task from the same distribution. This is achieved by the agent learning to effectively implement a fast RL-like algorithm in the *dynamics* of the network (Figure 5). This process, whereby an agent trained slowly on a large distribution of tasks can rapidly adapt to a new task, is known as ‘meta-reinforcement learning’ and is a popular area of research in machine learning (Finn et al., 2017; Ritter et al., 2018; Duan et al., 2016; Wang et al., 2016). Wang et al. (2018) showed that such a meta-RL model can explain a range of neuroscientific findings, including

- Dynamic adaptation of the effective learning rate of an agent to the volatility of the environment (Behrens et al., 2007).
- The emergence of ‘model-based’ behaviour in the ‘two-step’ task commonly used to distinguish between model-free and model-based RL (Miller et al., 2017; Daw et al., 2011).
- The ability of animals to get progressively faster at learning when exposed to multiple tasks with a consistent abstract task structure (Harlow, 1949).

Recently, Jensen et al. (2023) also extended the work of Wang et al. (2018) to allow the meta-RL agent to learn not just from physical experience, but also from imagined experience using a learned model of the environment. This resulted in an agent that computes an initial model-free policy, which can be adaptively improved with model-based computations when the resulting policy improvement makes up for the temporal opportunity cost of the model-based computation. Interestingly, the response times of the resulting agent mirrored those of human participants in a maze navigation task, where the agent similarly spent more time ‘thinking’ early in a trial and far from the goal.

Deep Q-learning

While the policy gradient methods discussed above are useful, they also have limitations. One is that most policy gradient methods are fundamentally ‘on-policy’, which means that the data used for learning must be sampled from the agent itself. This is necessary for the log derivative trick to work. Another is that the gradient can have fairly high variance despite all of our variance reduction efforts. We can begin to tackle both of these shortcomings using a method known as ‘deep Q-learning’. To do so, we first note that our actor-critic algorithm above required us to estimate the value function $V_\phi(s_t)$. However, as we saw in Equation 11, such value functions can directly be used for action selection without having to fit a separate policy network. We also noted previously that this requires simulating the results of the actions, which can be inconvenient. As in the tabular setting, we can circumvent this problem by directly fitting state-action values (‘Q-values’), now using function approximation. This gives rise to the family of ‘deep Q-learning’ methods, which closely mirror the tabular Q-learning considered previously, but now with function approximation.

The general recipe involves defining a Q function $Q_\theta(a, s)$, where the parameters θ of the deep network defining our agent are learned as follows:

- Collect experience (s_t, a_t, r_t, s_{t+1}) .
- Define a loss $\mathcal{L} = 0.5[Q_\theta(s_t, a_t) - (r_t + \gamma \max_a Q_\theta(s_{t+1}, a))]^2$.
- Update the network parameters $\Delta\theta \propto -\frac{\partial \mathcal{L}}{\partial \theta}$.

The above steps can either be run ‘online’ using the experience of the agent as it is being generated, or it could occur ‘in batch’, whereby a collection of experiences is first generated, followed by optimization of the

Q network. The ‘max’ in the target value ensures that we continuously improve our policy. When acting according to our policy, we simply pick the action predicted to have the highest value, usually using some variant of ϵ -greedy or softmax to introduce stochasticity and variability into our trajectories.

On the surface, the above looks like a straightforward generalization of tabular Q-learning, and it may seem surprising that deep Q-learning did not see significant use or success until the foundational work of [Mnih et al. \(2013\)](#). However, a major difficulty arises from the autocorrelation of the states observed by the agent, which leads to the network ‘chasing’ a target function $(r_t + \gamma \max_a Q_\theta(s_{t+1}, a))$ that changes with the environment. A critical advance that overcame the resulting instability was the use of an experience replay buffer, whereby the experience generated by the agent is added to a global replay buffer \mathcal{B} . One or more *random* experiences are then sampled from the buffer and used to update the network parameters – reminiscent of the ‘DYNA’ architecture described previously. An additional algorithmic instability arises from the fact that \mathcal{L} includes the term $\max_a Q_\theta(s_{t+1}, a)$, which we cannot take gradients through despite its dependence on θ . This means that we are trying to optimize our parameters for a continuously moving target, which destabilizes the optimization process. To combat this, it is common to use a ‘target network’ $Q_{\theta'}(s_{t+1}, a)$ that is fixed for a period of time, usually after being set to a copy of our ‘student network’. Together, these two approaches give rise to the ‘deep Q network’ (DQN) developed by [Mnih et al. \(2013\)](#), which is trained as follows:

- Collect experience (s_t, a_t, r_t, s_{t+1}) and add to \mathcal{B} [optionally many iterations].
- Sample a *new* experience $(s'_t, a'_t, r'_t, s'_{t+1}) \sim \mathcal{B}$ [optionally a full batch].
- Define a loss $\mathcal{L} = 0.5[Q_\theta(s'_t, a'_t) - (r'_t + \gamma \max_a Q_{\theta'}(s'_{t+1}, a))]^2$ [optionally averaged over the full batch]. Note that we are training the student network with parameters θ while using a target network with parameters θ' inside the max.
- Update the network parameters $\Delta\theta \propto -\frac{\partial \mathcal{L}}{\partial \theta}$.
- Once we have repeated the above a sufficient number of times, set our target network to the student network, $\theta' \leftarrow \theta$.

As indicated above, this procedure usually involves averaging over a full batch of experience when computing gradients. Experience can also be collected in batch, and usually ‘stale’ experiences are periodically removed from \mathcal{B} . It is worth noting that this algorithm is effectively off-policy, since most experience in \mathcal{B} was collected by a policy defined by an old set of parameters θ – and the data in \mathcal{B} can in fact be generated completely independently of the agent we are training. Finally, even though the above is more stable than naive deep Q-learning, an additional instability arises from the fact that $Q_{max}(s'_{t+1}) = \max_a Q_{\theta'}(s'_{t+1}, a)$ uses the same Q values both to estimate which action is best and what the value of that action is, which leads to a positively biased estimate. This can be mitigated by using *separate* Q networks to select the best action and evaluate its value, $Q_{max}(s'_{t+1}) \leftarrow Q_{\theta'}(s'_{t+1}, \arg\max_a(Q_\theta(s'_{t+1}, a)))$, in an approach known as ‘double Q-learning’ ([Van Hasselt et al., 2016](#)). Commonly, this is done by simply using the student network for action selection and the target network to evaluate its expected value.

While DQNs have shown impressive performance across a range of machine learning settings ([Mnih et al., 2013](#); [Lillicrap et al., 2015](#); [Schaul et al., 2015](#); [Kalashnikov et al., 2018](#)), they have seen less interest from the neuroscience community. This is perhaps paradoxical given the prevalence of tabular Q-learning in the theoretical neuroscience literature. An interesting exception to this is recent work by [Makino \(2023\)](#), which shows parallels between the values learned by a DQN and neural representations in mammalian cortex during a compositional behavioural task. Additionally, the importance of experience replay in DQNs ([Mnih et al., 2013](#); [Schaul et al., 2015](#)) has close parallels to the proposal that hippocampal replay constitutes a form of experience replay ([Mattar and Daw, 2018](#)) – although the latter was only analyzed in a tabular setting.

Distributional reinforcement learning

In Equation 3 and Equation 12, we defined the *expected* reward for a given state or state-action pair. The methods considered so far have only used such expectations as a learning signal. However, recent work has suggested that performance could be improved by learning the full *distribution* of cumulative future rewards for a given state-action pair (Bellemare et al., 2017, 2023; Dabney et al., 2018), a single sample of which we denote Z :

$$Z(s, a) \sim p \left(\sum_{t' \geq t} \gamma^{t'-t} r_{t'} \mid s_t = s, a_t = a \right) \quad (52)$$

The stochasticity of Z can both be due to stochasticity in environment dynamics and reward, and it can be due to stochasticity in the policy of the agent itself. Clearly, the expectation of samples of Z equal the corresponding Q value:

$$\mathbb{E}_{p(Z)} [Z(s, a)] = Q(s, a). \quad (53)$$

Instead of only estimating this expectation, we now want to learn the full distribution of returns under our policy π , $p_\pi(Z(s, a))$. One use of learning this distribution is to develop methods that are risk averse (Morimura et al., 2010, 2012) or explicitly take into account uncertainty (Dearden et al., 1998). However, recent work has suggested that such a distributional approach can also lead to improved performance in terms of expected rewards by improving representation learning in the deep RL setting (Bellemare et al., 2017; Dabney et al., 2018; Rowland et al., 2019; Bellemare et al., 2023). Some intuition for this can be had from noting that traditional deep RL approaches will only learn to distinguish states that have different expected value, while distributional RL will learn to distinguish any states that have different cumulative return distributions.

To learn $p_\pi(Z(s, a))$, one option is to define a set of ‘atoms’ that tile the (expected) support of the distribution and then discretize the distribution by assigning the full probability mass to these discrete locations. An approximate $p_\pi(Z(s, a))$ can then be iteratively improved using temporal differences by propagating each atom through the Bellman equation (Equation 15), projecting the density back onto the discretized locations, and training an RL agent to predict the corresponding probabilities. This is the approach originally employed by Bellemare et al. (2017). However, it turns out to be more convenient from a neuroscientific perspective to represent a different set of sufficient statistics for $p_\pi(Z(s, a))$ (Dabney et al., 2020; Lowet et al., 2020). We do this by defining the τ^{th} *expectile* of $p_\pi(Z(s, a))$, ϵ_τ , which is defined for a random variable Z as the solution to the equation

$$\tau \mathbb{E}[\max(0, Z - \epsilon_\tau)] = (1 - \tau) \mathbb{E}[\max(0, \epsilon_\tau - Z)]. \quad (54)$$

This is a generalization of the mean, which is recovered for $\tau = 0.5$, and is similar to how the quantile generalizes the notion of a median. A distribution is uniquely specified by its expectiles, and we can therefore represent $p_\pi(Z(s, a))$ in terms of $\{\epsilon_\tau\}$. Translating this to an RL algorithm involves training a network (or tabular values) to predict a set of expectiles for a given state (and action). The parameters of the agent are then updated by propagating the distribution implied by the predicted expectiles through the Bellman equation and minimizing the difference between the initial and propagated distributions.

In the tabular value learning case (c.f. Section 3), this turns out to be particularly simple do via the use of a modified TD-update rule (c.f. Equation 9; Lowet et al., 2020; Figure 6A). In particular, we consider a set of units $\{V_i(s)\}$, each with a target expectile $\tau_i := \frac{\alpha_i^+}{\alpha_i^+ + \alpha_i^-}$ of the return distribution $p_\pi(Z(s))$ (where $Z(s) = \mathbb{E}_{a \sim \pi(a|s)} [Z(a, s)]$). These expectiles can be learned by sampling experience from the environment under the policy and defining a TD error for each unit and state transition as

$$\delta_i := r_t + \gamma \tilde{Z}_j(s_{t+1}) - V_i(s_t). \quad (55)$$

Here, $\tilde{Z}_j(s_{t+1})$ is a *random sample* from the learned approximate distribution of cumulative future returns from state s_{t+1} , $p_{\{V_i\}}(\tilde{Z}(s_{t+1}))$ (Lowet et al., 2020; Dabney et al., 2020). We then apply the following update rule to all units:

$$\Delta V_i(s_t) = \alpha_i^+ \max(\delta_i, 0) + \alpha_i^- \min(\delta_i, 0). \quad (56)$$

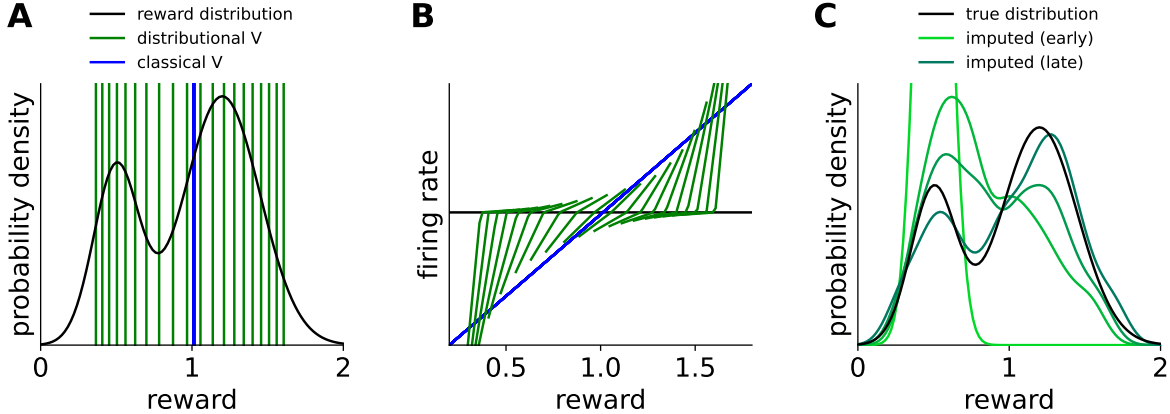


Figure 6: **Distributional reinforcement learning.** The results in this figure reproduce some of the key simulations of Dabney et al. (2020). These simulations were all run on a simple value estimation task with a single state and no actions. (A) Distribution of rewards (black), plotted together with the values V_i converged to across 20 units all learning through standard TD learning (blue), or through distributional RL with different $\tau_i = \frac{\alpha_i^+}{\alpha_i^+ + \alpha_i^-}$ (green). The TD units all converge to the mean reward, while the expectile units end up tiling the distribution. (B) For both the TD units and distributional units from (A), we plot the temporal difference updates performed in response to different rewards from the reward distribution. These updates have been proposed to be represented in the firing rates of dopaminergic VTA neurons relative to baseline (Schultz et al., 1997; Dabney et al., 2020). The TD units show a constant linear scaling across positive and negative rewards, while the distributional units show an asymmetric scaling of firing rate with reward magnitude above and below their reversal point (black horizontal line). The ratio of slopes above and below the reversal point scales positively with the value of the reversal point. These features of dopaminergic VTA neurons were used by Dabney et al. (2020) to argue that the brain implements a form of distributional RL. (C) True reward distribution (black) reproduced from (A), now plotted together with the reward distribution $p_{\{V_i\}}(\tilde{Z})$ implied by the distributional units from (A) and (B) at different stages of learning (light to dark green). These imputed distributions were computed by assuming that the value V_i learned by unit i corresponds to expectile $\tau_i = \frac{\alpha_i^+}{\alpha_i^+ + \alpha_i^-}$ of the reward distribution. We then impute the distribution implied by these expectiles under the assumption that it consists of a set of N delta functions in the case of N expectiles (Rowland et al., 2019). Finally, we convolved the resulting delta functions with a Gaussian kernel ($\sigma = 0.1$) for visualization. This whole process was repeated using $\{V_i\}$ at different stages of learning. The units were all initialized at $V_i = 0.5$, so the initial distribution is a delta function at $r = 0.5$. At the end of learning, the population faithfully represents the true reward distribution, capturing key features including bimodality and the relative magnitude of the two modes. Dabney et al. (2020) used a similar approach to infer the distribution implicitly encoded by dopaminergic VTA neurons at the end of animal training and found a close match to the true reward distribution.

In other words, we apply the TD update rule to each unit with learning rate α_i^+ for positive TD errors and learning rate α_i^- for negative TD errors. When running this algorithm to convergence, $V_i(s)$ will approach the τ_i^{th} expectile (ϵ_{τ_i}) of $p_\pi(Z(s))$. In the deep RL setting, we would additionally use the chain rule to multiply $\Delta V_i(s_t)$ from Equation 56 by $\partial V_i(s_t)/\partial \theta$ and sum over i to learn a model with parameters θ that can predict the full set of expectiles. Another variant of this algorithm updates each unit with $\alpha_i \text{sign}(\delta_i)$ instead of $\alpha_i(\delta_i)$, which leads to learning of the τ_i^{th} quartiles of the distribution instead of the expectiles. We refer to Bellemare et al. (2017); Dabney et al. (2018); Rowland et al. (2019); Bellemare et al. (2023); and Dabney et al. (2020) for additional mathematical details and extensions to the control setting.

Intriguingly, recent work in neuroscience has suggested that a similar algorithm could potentially underlie value learning in biological neural circuits (Dabney et al., 2020; Lowet et al., 2020). In particular, Dabney et al. (2020) recorded the activity of dopaminergic VTA neurons during a task with stochastic rewards and showed that the neurons appeared to represent the full distribution of possible outcomes using an expectile

representation as described above. More concretely, they showed that:

- The VTA neurons exhibited a range of different ‘reversal points’ – defined as the reward magnitude at which the firing rate of a neuron did not change from its baseline firing rate. This is consistent with a distributional RL theory, where the changes in neural firing rates from baseline correspond to the expectile TD updates considered above. In this case, the reversal point of a neuron i should be $V_i \approx \epsilon_{\tau_i}$ (Figure 6B).
- Neurons had different slopes describing the relationship between expected reward and firing rate in the regimes where expected reward was above and below the reversal point (V_i) of each neuron. This is consistent with the algorithm described in Equation 56 (Figure 6B).
- When independently fitting a slope to the data above (α_i^+) and below (α_i^-) the reversal point of neuron i , the reversal point of the neuron was positively correlated with $\tau_i = \frac{\alpha_i^+}{\alpha_i^- + \alpha_i^+}$. This is consistent with the expectile distributional RL setting, where the reversal point is $V_i \approx \epsilon_{\tau_i}$ (Figure 6B).
- When ‘imputing’ the distribution (approximated as a set of delta functions) implied by the VTA neurons when interpreted as expectiles (Figure 6C), the resulting fit was remarkably similar to the true distribution of rewards in the experiment.

These findings generalize the canonical RPE view of Schultz et al. (1997), which can be seen as the averaged version of the theory put forward by Dabney et al. (2020). The expectile regression algorithm investigated by Dabney et al. (2020) relies on non-local TD updates and non-linear ‘imputation’ of the return distribution $p_{\{V_i\}}(\tilde{Z}(s))$ induced by the learned expectiles $\{V_i(s)\}$. However, recent work has suggested more biologically plausible distributional RL updates that are also consistent with the biological data (Tano et al., 2020).

8 Discussion

In this work, we have provided a mathematical overview of some of the many reinforcement learning methods that are commonly used in systems and computational neuroscience. We have also highlighted a range of explicit parallels between these methods and findings in the neuroscience and cognitive science literature to illustrate the utility of reinforcement learning as a framework for understanding biological learning and decision making. This has ranged from classical work on reward prediction errors (Schultz et al., 1997) to recent findings on the plausibility of distributional reinforcement learning in biological circuits (Dabney et al., 2020).

While RL has thus already had a profound influence on systems neuroscience, several open questions remain. In particular, much of the work in neuroscience has focused on simple stimulus-response or binary decision making tasks. This is a far reach from ethologically relevant problems that involve processing complex multimodal stimuli, decision making with long-lasting consequences, and complex high-dimensional motor control. Some recent work building on deep RL has started to bridge this gap. For example, Banino et al. (2018) showed the emergence of grid cells in agents navigating complex environments, Merel et al. (2019) showed similarities between an RL agent trained on a suite of complex motor tasks and rodent motor representations, and Jensen et al. (2023) showed parallels between a recurrent meta-RL agent and human behaviour in a navigation task requiring temporally extended thinking. However, much work remains to be done to extend our neuroscientific findings to ethologically relevant settings, both on the experimental side and on the computational side.

A related challenge will be to combine different components of existing models to capture the generalist nature of biological circuits. This is in contrast to past work, which has often focused on a single neural circuit or function, such as motor control or navigation. Such a generalist approach will involve explicit modeling of the roles of different brain regions, and more importantly it will require us to capture how they interact with one another during learning and decision making. Clearly, such models will need to be constrained by experimental data, both at the level of behaviour and at the level of neural activity. This

is becoming increasingly feasible with recent advances in recording technologies, both for high-resolution behavioural tracking (Mathis et al., 2018; Dunn et al., 2021) and for simultaneous and long-term recording of neural activity (Steinmetz et al., 2021; Pachitariu et al., 2016; Dhawale et al., 2017).

Finally, most work on reinforcement learning in a neuroscientific context has considered short-term decision making tasks, where planning and decision making in primitive state and action spaces is feasible. This is in stark contrast to most human decision making, which occurs over extended timescales and often involves hierarchies of decisions. For example, we may decide to pursue an undergraduate degree at Cambridge University, which then requires us to (i) write an application, (ii) prepare for an interview, and (iii) arrange our travel. Each of these processes in turn require us to plan increasingly low-level decisions, such as booking a flight or deciding which bus to take to the airport. This is the topic of hierarchical reinforcement learning, which has already been highlighted as a potentially useful model of human behaviour (Eckstein and Collins, 2020; Botvinick, 2008; Botvinick et al., 2009) and is becoming an increasingly important area of research in machine learning (Pateria et al., 2021).

As is the case for hierarchical RL, this review has unfortunately not been able to cover in detail all topics in reinforcement learning that are of interest to neuroscientists. A brief overview of this and additional topics of interest is therefore provided in Section 9, which we hope can also serve as a useful pointer to the broader reinforcement learning literature and some of the active research topics being pursued by the community.

References

- Agrawal, M., Mattar, M. G., Cohen, J. D., and Daw, N. D. (2022). The temporal dynamics of opportunity costs: A normative account of cognitive fatigue and boredom. *Psychological review*, 129(3):564.
- Akam, T., Costa, R., and Dayan, P. (2015). Simple plans or sophisticated habits? state, transition and learning interactions in the two-step task. *PLoS computational biology*, 11(12):e1004648.
- Alvernhe, A., Save, E., and Poucet, B. (2011). Local remapping of place cell firing in the tolmán detour task. *European Journal of Neuroscience*, 33(9):1696–1705.
- Banino, A., Barry, C., Uria, B., Blundell, C., Lillicrap, T., Mirowski, P., Pritzel, A., Chadwick, M. J., Degrís, T., Modayil, J., et al. (2018). Vector-based navigation using grid-like representations in artificial agents. *Nature*, 557(7705):429–433.
- Barreto, A., Dabney, W., Munos, R., Hunt, J. J., Schaul, T., van Hasselt, H. P., and Silver, D. (2017). Successor features for transfer in reinforcement learning. *Advances in neural information processing systems*, 30.
- Behrens, T. E., Woolrich, M. W., Walton, M. E., and Rushworth, M. F. (2007). Learning the value of information in an uncertain world. *Nature neuroscience*, 10(9):1214–1221.
- Bellemare, M. G., Dabney, W., and Munos, R. (2017). A distributional perspective on reinforcement learning. In *International conference on machine learning*, pages 449–458. PMLR.
- Bellemare, M. G., Dabney, W., and Rowland, M. (2023). *Distributional reinforcement learning*. MIT Press.
- Blanco-Pozo, M., Akam, T., and Walton, M. (2021). Dopamine reports reward prediction errors, but does not update policy, during inference-guided choice. *bioRxiv*.
- Botvinick, M. and Toussaint, M. (2012). Planning as inference. *Trends in cognitive sciences*, 16(10):485–488.
- Botvinick, M., Wang, J. X., Dabney, W., Miller, K. J., and Kurth-Nelson, Z. (2020). Deep reinforcement learning and its neuroscientific implications. *Neuron*, 107(4):603–616.
- Botvinick, M. M. (2008). Hierarchical models of behavior and prefrontal function. *Trends in cognitive sciences*, 12(5):201–208.

- Botvinick, M. M. and Cohen, J. D. (2014). The computational and neural basis of cognitive control: charted territory and new frontiers. *Cognitive science*, 38(6):1249–1285.
- Botvinick, M. M., Niv, Y., and Barto, A. G. (2009). Hierarchically organized behavior and its neural foundations: A reinforcement learning perspective. *cognition*, 113(3):262–280.
- Callaway, F., van Opheusden, B., Gul, S., Das, P., Krueger, P. M., Griffiths, T. L., and Lieder, F. (2022). Rational use of cognitive resources in human planning. *Nature Human Behaviour*, 6(8):1112–1125.
- Clavera, I., Fu, V., and Abbeel, P. (2020). Model-augmented actor-critic: Backpropagating through paths. *arXiv preprint arXiv:2005.08068*.
- Dabney, W., Kurth-Nelson, Z., Uchida, N., Starkweather, C. K., Hassabis, D., Munos, R., and Botvinick, M. (2020). A distributional code for value in dopamine-based reinforcement learning. *Nature*, 577(7792):671–675.
- Dabney, W., Rowland, M., Bellemare, M., and Munos, R. (2018). Distributional reinforcement learning with quantile regression. In *Proceedings of the AAAI Conference on Artificial Intelligence*, volume 32.
- Daw, N. D., Gershman, S. J., Seymour, B., Dayan, P., and Dolan, R. J. (2011). Model-based influences on humans’ choices and striatal prediction errors. *Neuron*, 69(6):1204–1215.
- Daw, N. D., Niv, Y., and Dayan, P. (2005). Uncertainty-based competition between prefrontal and dorso-lateral striatal systems for behavioral control. *Nature neuroscience*, 8(12):1704–1711.
- Dayan, P. (1993). Improving generalization for temporal difference learning: The successor representation. *Neural computation*, 5(4):613–624.
- Dearden, R., Friedman, N., and Russell, S. (1998). Bayesian q-learning. *Aaai/iaai*, 1998:761–768.
- Deisenroth, M. and Rasmussen, C. E. (2011). Pilco: A model-based and data-efficient approach to policy search. In *Proceedings of the 28th International Conference on machine learning (ICML-11)*, pages 465–472.
- Dhawale, A. K., Poddar, R., Wolff, S. B., Normand, V. A., Kopelowitz, E., and Ölveczky, B. P. (2017). Automated long-term recording and analysis of neural activity in behaving animals. *Elife*, 6:e27702.
- Duan, Y., Schulman, J., Chen, X., Bartlett, P. L., Sutskever, I., and Abbeel, P. (2016). RL2: Fast reinforcement learning via slow reinforcement learning. *arXiv preprint arXiv:1611.02779*.
- Dunn, T. W., Marshall, J. D., Severson, K. S., Aldarondo, D. E., Hildebrand, D. G., Chettih, S. N., Wang, W. L., Gellis, A. J., Carlson, D. E., Aronov, D., et al. (2021). Geometric deep learning enables 3d kinematic profiling across species and environments. *Nature methods*, 18(5):564–573.
- Eckstein, M. K. and Collins, A. G. (2020). Computational evidence for hierarchically structured reinforcement learning in humans. *Proceedings of the National Academy of Sciences*, 117(47):29381–29389.
- Finn, C., Abbeel, P., and Levine, S. (2017). Model-agnostic meta-learning for fast adaptation of deep networks. In *International conference on machine learning*, pages 1126–1135. PMLR.
- Geerts, J. P., Chersi, F., Stachenfeld, K. L., and Burgess, N. (2020). A general model of hippocampal and dorsal striatal learning and decision making. *Proceedings of the National Academy of Sciences*, 117(49):31427–31437.
- Gershman, S. J. (2018). The successor representation: its computational logic and neural substrates. *Journal of Neuroscience*, 38(33):7193–7200.
- Griffiths, T. L., Callaway, F., Chang, M. B., Grant, E., Krueger, P. M., and Lieder, F. (2019). Doing more with less: meta-reasoning and meta-learning in humans and machines. *Current Opinion in Behavioral Sciences*, 29:24–30.

- Gronauer, S. and Diepold, K. (2022). Multi-agent deep reinforcement learning: a survey. *Artificial Intelligence Review*, pages 1–49.
- Haarnoja, T., Zhou, A., Hartikainen, K., Tucker, G., Ha, S., Tan, J., Kumar, V., Zhu, H., Gupta, A., Abbeel, P., et al. (2018). Soft actor-critic algorithms and applications. *arXiv preprint arXiv:1812.05905*.
- Harlow, H. F. (1949). The formation of learning sets. *Psychological review*, 56(1):51.
- Hart, P. E., Nilsson, N. J., and Raphael, B. (1968). A formal basis for the heuristic determination of minimum cost paths. *IEEE transactions on Systems Science and Cybernetics*, 4(2):100–107.
- Jaderberg, M., Mnih, V., Czarnecki, W. M., Schaul, T., Leibo, J. Z., Silver, D., and Kavukcuoglu, K. (2016). Reinforcement learning with unsupervised auxiliary tasks. *arXiv preprint arXiv:1611.05397*.
- Jensen, K. T., Hennequin, G., and Mattar, M. G. (2023). A recurrent network model of planning explains hippocampal replay and human behavior. *bioRxiv*, pages 2023–01.
- Kalashnikov, D., Irpan, A., Pastor, P., Ibarz, J., Herzog, A., Jang, E., Quillen, D., Holly, E., Kalakrishnan, M., Vanhoucke, V., et al. (2018). Qt-opt: Scalable deep reinforcement learning for vision-based robotic manipulation. *arXiv preprint arXiv:1806.10293*.
- Keramati, M., Smittenaar, P., Dolan, R. J., and Dayan, P. (2016). Adaptive integration of habits into depth-limited planning defines a habitual-goal-directed spectrum. *Proceedings of the National Academy of Sciences*, 113(45):12868–12873.
- Killcross, S. and Coutureau, E. (2003). Coordination of actions and habits in the medial prefrontal cortex of rats. *Cerebral cortex*, 13(4):400–408.
- Lai, L. and Gershman, S. J. (2021). Policy compression: An information bottleneck in action selection. In *Psychology of Learning and Motivation*, volume 74, pages 195–232. Elsevier.
- Lengyel, M. and Dayan, P. (2007). Hippocampal contributions to control: the third way. *Advances in neural information processing systems*, 20.
- Levine, S. (2018). Reinforcement learning and control as probabilistic inference: Tutorial and review. *arXiv preprint arXiv:1805.00909*.
- Levine, S., Kumar, A., Tucker, G., and Fu, J. (2020). Offline reinforcement learning: Tutorial, review, and perspectives on open problems. *arXiv preprint arXiv:2005.01643*.
- Li, C., Kreiman, G., and Ramanathan, S. (2022). Integrating artificial and biological neural networks to improve animal task performance using deep reinforcement learning. *bioRxiv*, pages 2022–09.
- Lillicrap, T. P., Hunt, J. J., Pritzel, A., Heess, N., Erez, T., Tassa, Y., Silver, D., and Wierstra, D. (2015). Continuous control with deep reinforcement learning. *arXiv preprint arXiv:1509.02971*.
- Loukola, O. J., Solvi, C., Coscos, L., and Chittka, L. (2017). Bumblebees show cognitive flexibility by improving on an observed complex behavior. *Science*, 355(6327):833–836.
- Lowet, A. S., Zheng, Q., Matias, S., Drugowitsch, J., and Uchida, N. (2020). Distributional reinforcement learning in the brain. *Trends in neurosciences*, 43(12):980–997.
- Makino, H. (2023). Arithmetic value representation for hierarchical behavior composition. *Nature Neuroscience*, 26(1):140–149.
- Mathis, A., Mamidanna, P., Cury, K. M., Abe, T., Murthy, V. N., Mathis, M. W., and Bethge, M. (2018). Deeplabcut: markerless pose estimation of user-defined body parts with deep learning. *Nature neuroscience*, 21(9):1281–1289.
- Mattar, M. G. and Daw, N. D. (2018). Prioritized memory access explains planning and hippocampal replay. *Nature neuroscience*, 21(11):1609–1617.

- Mehta, M. R., Quirk, M. C., and Wilson, M. A. (2000). Experience-dependent asymmetric shape of hippocampal receptive fields. *Neuron*, 25(3):707–715.
- Merel, J., Aldarondo, D., Marshall, J., Tassa, Y., Wayne, G., and Ölveczky, B. (2019). Deep neuroethology of a virtual rodent. *arXiv preprint arXiv:1911.09451*.
- Miller, K. J., Botvinick, M. M., and Brody, C. D. (2017). Dorsal hippocampus contributes to model-based planning. *Nature neuroscience*, 20(9):1269–1276.
- Mizes, K. G., Lindsey, J., Escola, G. S., and Ölveczky, B. P. (2023a). Dissociating the contributions of sensorimotor striatum to automatic and visually guided motor sequences. *Nature Neuroscience*, pages 1–14.
- Mizes, K. G., Lindsey, J., Escola, G. S., and Ölveczky, B. P. (2023b). Motor cortex is required for flexible but not automatic motor sequences. *bioRxiv*, pages 2023–09.
- Mnih, V., Kavukcuoglu, K., Silver, D., Graves, A., Antonoglou, I., Wierstra, D., and Riedmiller, M. (2013). Playing atari with deep reinforcement learning. *arXiv preprint arXiv:1312.5602*.
- Momennejad, I., Russek, E. M., Cheong, J. H., Botvinick, M. M., Daw, N. D., and Gershman, S. J. (2017). The successor representation in human reinforcement learning. *Nature human behaviour*, 1(9):680–692.
- Morimura, T., Sugiyama, M., Kashima, H., Hachiya, H., and Tanaka, T. (2010). Nonparametric return distribution approximation for reinforcement learning. In *Proceedings of the 27th International Conference on Machine Learning (ICML-10)*, pages 799–806.
- Morimura, T., Sugiyama, M., Kashima, H., Hachiya, H., and Tanaka, T. (2012). Parametric return density estimation for reinforcement learning. *arXiv preprint arXiv:1203.3497*.
- Morris, G., Nevet, A., Arkadir, D., Vaadia, E., and Bergman, H. (2006). Midbrain dopamine neurons encode decisions for future action. *Nature neuroscience*, 9(8):1057–1063.
- Niv, Y. (2009). Reinforcement learning in the brain. *Journal of Mathematical Psychology*, 53(3):139–154.
- Nowé, A., Vrancx, P., and De Hauwere, Y.-M. (2012). Game theory and multi-agent reinforcement learning. *Reinforcement Learning: State-of-the-Art*, pages 441–470.
- Olds, J. and Milner, P. (1954). Positive reinforcement produced by electrical stimulation of septal area and other regions of rat brain. *Journal of comparative and physiological psychology*, 47(6):419.
- Pachitariu, M., Stringer, C., Schröder, S., Dipoppa, M., Rossi, L. F., Carandini, M., and Harris, K. D. (2016). Suite2p: beyond 10,000 neurons with standard two-photon microscopy. *BioRxiv*, page 061507.
- Pan, Y., Cheng, C.-A., Saigol, K., Lee, K., Yan, X., Theodorou, E., and Boots, B. (2017). Agile autonomous driving using end-to-end deep imitation learning. *arXiv preprint arXiv:1709.07174*.
- Pateria, S., Subagdja, B., Tan, A.-h., and Quek, C. (2021). Hierarchical reinforcement learning: A comprehensive survey. *ACM Computing Surveys (CSUR)*, 54(5):1–35.
- Piray, P. and Daw, N. D. (2021). Linear reinforcement learning in planning, grid fields, and cognitive control. *Nature communications*, 12(1):1–20.
- Rao, R. P. and Ballard, D. H. (1999). Predictive coding in the visual cortex: a functional interpretation of some extra-classical receptive-field effects. *Nature neuroscience*, 2(1):79–87.
- Ritter, S., Wang, J., Kurth-Nelson, Z., Jayakumar, S., Blundell, C., Pascanu, R., and Botvinick, M. (2018). Been there, done that: Meta-learning with episodic recall. In *International conference on machine learning*, pages 4354–4363. PMLR.
- Roesch, M. R., Calu, D. J., and Schoenbaum, G. (2007). Dopamine neurons encode the better option in rats deciding between differently delayed or sized rewards. *Nature neuroscience*, 10(12):1615–1624.

- Rowland, M., Dadashi, R., Kumar, S., Munos, R., Bellemare, M. G., and Dabney, W. (2019). Statistics and samples in distributional reinforcement learning. In *International Conference on Machine Learning*, pages 5528–5536. PMLR.
- Schaul, T., Quan, J., Antonoglou, I., and Silver, D. (2015). Prioritized experience replay. *arXiv preprint arXiv:1511.05952*.
- Schrittwieser, J., Antonoglou, I., Hubert, T., Simonyan, K., Sifre, L., Schmitt, S., Guez, A., Lockhart, E., Hassabis, D., Graepel, T., et al. (2020). Mastering atari, go, chess and shogi by planning with a learned model. *Nature*, 588(7839):604–609.
- Schultz, W., Dayan, P., and Montague, P. R. (1997). A neural substrate of prediction and reward. *Science*, 275(5306):1593–1599.
- Silver, D., Hubert, T., Schrittwieser, J., Antonoglou, I., Lai, M., Guez, A., Lanctot, M., Sifre, L., Kumaran, D., Graepel, T., et al. (2018). A general reinforcement learning algorithm that masters chess, shogi, and go through self-play. *Science*, 362(6419):1140–1144.
- Solway, A. and Botvinick, M. M. (2012). Goal-directed decision making as probabilistic inference: a computational framework and potential neural correlates. *Psychological review*, 119(1):120.
- Stachenfeld, K. L., Botvinick, M. M., and Gershman, S. J. (2017). The hippocampus as a predictive map. *Nature neuroscience*, 20(11):1643–1653.
- Steinmetz, N. A., Aydin, C., Lebedeva, A., Okun, M., Pachitariu, M., Bauza, M., Beau, M., Bhagat, J., Böhm, C., Broux, M., et al. (2021). Neuropixels 2.0: A miniaturized high-density probe for stable, long-term brain recordings. *Science*, 372(6539):eabf4588.
- Sutton, R. S. (1991). Dyna, an integrated architecture for learning, planning, and reacting. *ACM Sigart Bulletin*, 2(4):160–163.
- Sutton, R. S. and Barto, A. G. (2018). *Reinforcement learning: An introduction*. MIT press.
- Sutton, R. S., Precup, D., and Singh, S. (1999). Between mdps and semi-mdps: A framework for temporal abstraction in reinforcement learning. *Artificial intelligence*, 112(1-2):181–211.
- Takahashi, Y., Schoenbaum, G., and Niv, Y. (2008). Silencing the critics: understanding the effects of cocaine sensitization on dorsolateral and ventral striatum in the context of an actor/critic model. *Frontiers in neuroscience*, 2:282.
- Tano, P., Dayan, P., and Pouget, A. (2020). A local temporal difference code for distributional reinforcement learning. *Advances in neural information processing systems*, 33:13662–13673.
- Todorov, E. (2006). Linearly-solvable markov decision problems. *Advances in neural information processing systems*, 19.
- Todorov, E. (2009). Efficient computation of optimal actions. *Proceedings of the national academy of sciences*, 106(28):11478–11483.
- Tsai, H.-C., Zhang, F., Adamantidis, A., Stuber, G. D., Bonci, A., De Lecea, L., and Deisseroth, K. (2009). Phasic firing in dopaminergic neurons is sufficient for behavioral conditioning. *Science*, 324(5930):1080–1084.
- Van Hasselt, H., Guez, A., and Silver, D. (2016). Deep reinforcement learning with double q-learning. In *Proceedings of the AAAI conference on artificial intelligence*, volume 30.
- Vértes, E. and Sahani, M. (2019). A neurally plausible model learns successor representations in partially observable environments. *Advances in Neural Information Processing Systems*, 32.

- Vikbladh, O. M., Meager, M. R., King, J., Blackmon, K., Devinsky, O., Shohamy, D., Burgess, N., and Daw, N. D. (2019). Hippocampal contributions to model-based planning and spatial memory. *Neuron*, 102(3):683–693.
- Vinyals, O., Babuschkin, I., Czarnecki, W. M., Mathieu, M., Dudzik, A., Chung, J., Choi, D. H., Powell, R., Ewalds, T., Georgiev, P., et al. (2019). Grandmaster level in StarCraft II using multi-agent reinforcement learning. *Nature*, 575(7782):350–354.
- Vul, E., Goodman, N., Griffiths, T. L., and Tenenbaum, J. B. (2014). One and done? optimal decisions from very few samples. *Cognitive science*, 38(4):599–637.
- Wang, J. X., Kurth-Nelson, Z., Kumaran, D., Tirumala, D., Soyer, H., Leibo, J. Z., Hassabis, D., and Botvinick, M. (2018). Prefrontal cortex as a meta-reinforcement learning system. *Nature neuroscience*, 21(6):860–868.
- Wang, J. X., Kurth-Nelson, Z., Tirumala, D., Soyer, H., Leibo, J. Z., Munos, R., Blundell, C., Kumaran, D., and Botvinick, M. (2016). Learning to reinforcement learn. *arXiv preprint arXiv:1611.05763*.
- Watkins, C. J. and Dayan, P. (1992). Q-learning. *Machine learning*, 8:279–292.
- Watkins, C. J. C. H. (1989). Learning from delayed rewards.
- Whittington, J. C., Muller, T. H., Mark, S., Chen, G., Barry, C., Burgess, N., and Behrens, T. E. (2020). The Tolman-Eichenbaum machine: unifying space and relational memory through generalization in the hippocampal formation. *Cell*, 183(5):1249–1263.
- Williams, R. J. (1992). Simple statistical gradient-following algorithms for connectionist reinforcement learning. *Machine learning*, 8:229–256.
- Wurman, P. R., Barrett, S., Kawamoto, K., MacGlashan, J., Subramanian, K., Walsh, T. J., Capobianco, R., Devlic, A., Eckert, F., Fuchs, F., et al. (2022). Outracing champion Gran Turismo drivers with deep reinforcement learning. *Nature*, 602(7896):223–228.
- Yin, H. H., Knowlton, B. J., and Balleine, B. W. (2004). Lesions of dorsolateral striatum preserve outcome expectancy but disrupt habit formation in instrumental learning. *European journal of neuroscience*, 19(1):181–189.
- Yin, H. H., Ostlund, S. B., Knowlton, B. J., and Balleine, B. W. (2005). The role of the dorsomedial striatum in instrumental conditioning. *European Journal of Neuroscience*, 22(2):513–523.
- Zintgraf, L., Shiarlis, K., Igl, M., Schulze, S., Gal, Y., Hofmann, K., and Whiteson, S. (2019). VariBAD: A very good method for bayes-adaptive deep RL via meta-learning. *arXiv preprint arXiv:1910.08348*.

9 Additional topics of interest

While we have tried to provide a fairly comprehensive overview of topics in reinforcement learning of interest to neuroscience, there are naturally many interesting areas that we have had to omit. Here we provide a brief description of some of these together with pointers to relevant literature for those who are interested in exploring them further.

9.1 Auxiliary losses

A key challenge in deep reinforcement learning is that of ‘representation learning’ (Botvinick et al., 2020). In particular, because rewards are generally sparse, it can be difficult to learn the full processing pipeline from raw inputs to a latent representation conducive to action selection on the basis of rewards alone. It is therefore common in the machine learning literature to introduce additional ‘auxiliary costs’ to the RL utility function, which use a richer data source to drive learning in the network. A common example is to include predictive losses that require the agent to predict the next observation from the current state and action (Jaderberg et al., 2016; Zintgraf et al., 2019). Such predictive losses have close parallels in neuroscience, where it has been suggested that predictive learning could result in many of the representations observed in biological circuits (Rao and Ballard, 1999; Stachenfeld et al., 2017; Whittington et al., 2020; Blanco-Pozo et al., 2021) and serve as a foundation for model-based planning (Jensen et al., 2023). This suggests a potentially important interaction between self-supervised representation learning and reward-driven reinforcement learning in biological circuits.

9.2 Hierarchical reinforcement learning

So far, we have considered a simple environment consisting of states and actions, and all planning and decision making has taken place in the space of action primitives. However, when planning over longer horizons, it can be necessary to break down the overall policy into a series of sub-goals, sub-policies, or ‘skills’ (Sutton et al., 1999; Pateria et al., 2021). This is the topic of hierarchical reinforcement learning (HRL) and ‘options’, where an agent learns a high-level policy over policies that can themselves be specified in terms of primitive actions or even lower-level policies. Such HRL has been found to explain features of human behaviour (Eckstein and Collins, 2020; Botvinick, 2008; Botvinick et al., 2009) and remains an area of substantial interest in the neuroscience literature.

9.3 Off-policy & offline reinforcement learning

In most of the work considered in this paper, the experience used to train the RL agents has been sampled from the policy of the agent itself. Indeed this is required for the gradients to be unbiased in the policy-gradient setting. However, an area of substantial interest is that of offline reinforcement learning, where the agent is trained from scratch on the basis of pre-collected experience (Levine et al., 2020). This is particularly important in cases where online data collection is expensive or too risky but large-scale datasets exist, such as in many healthcare settings. Off-policy reinforcement learning is the related problem of learning from a combination of online data and pre-generated data, possibly from a ‘stale’ version of the current agent. The off-policy setting is especially relevant to biology, where data collection is expensive and we therefore wish to make maximum use of existing data. This can e.g. be achieved through experience replay, which can be prioritized (instead of sampled at random) to maximize future reward and minimize temporal opportunity costs (Matar and Daw, 2018; Agrawal et al., 2022; Schaul et al., 2015).

9.4 Imitation learning

Related to the problem of offline reinforcement learning is that of *imitation learning*, where we also learn from pre-collected data. However, in contrast to offline RL where we make no assumption about the quality

of the policy used to collect the data, imitation learning assumes that the data has been collected by an ‘expert’ we wish to imitate (Levine et al., 2020). This is useful in cases where a large amount of expert data is available, such as the case of autonomous driving (Pan et al., 2017). Imitation learning is clearly important during early development in biological organisms, where we learn from observing the individuals around us. Indeed, such imitation learning is a hallmark not just of humans but has also been demonstrated in organisms as ‘simple’ as the bumblebee (Loukola et al., 2017).

9.5 Linear reinforcement learning

As we have seen in most of this tutorial, reinforcement learning is generally difficult and requires iterative algorithms that often scale poorly with the problem size. However, there are settings where we can simplify the problem to the point where it becomes analytically tractable in an approach known as ‘linear reinforcement learning’ (Todorov, 2006, 2009). This is similar to the SR approach, where we saw that the value function reduces to a linear function of the reward-per-state. Similar to how the SR matrix can be seen as describing the dynamics of some ‘base policy’, we also define a base policy in linear RL and compute a ‘control cost’ as the KL divergence between transition dynamics with and without our controller:

$$\mathcal{L}_{ctrl}(s) = KL[u(s'|s)||p(s'|s)], \quad (57)$$

where $p(s'|s)$ are the prior transition dynamics and $u(s'|s)$ are the controlled transition dynamics marginalized over the policy. For $\mathcal{L}_{ctrl}(s)$ to be well-defined, we require $u(s'|s) = 0$ whenever $p(s'|s) = 0$, which prevents impossible transitions even under our flexible controller. When subtracting this loss from the RL objective, the resulting utility turns out to be convex in u and can therefore be solved efficiently for the controller, which implicitly specifies the policy. This approach has recently been used as an explicit model of biological decision making (Piray and Daw, 2021). It also has close parallels to learning and planning as inference (Levine, 2018; Solway and Botvinick, 2012; Botvinick and Toussaint, 2012) and to RL with information bottlenecks (Lai and Gershman, 2021). Both of these families of approaches also involve reinforcement learning with a KL-regularized reward function, and they have also been used as models of biological decision making.

9.6 Successor features

In Section 6, we saw that the successor representation can be used as the basis of decision making that flexibly adapts to environments with changing reward structures. However, we developed this framework only in the tabular setting despite extending TD-learning and Q-learning to the ‘deep RL’ setting with function approximation. This leaves open the question of whether a similar generalization of the SR exists. This turns out to be the case and is known as ‘successor features’ (SF; Barreto et al., 2017), where the expected future observation of a given feature of the environment is used in place of the expected future state occupancy. Successor features have also been shown to have a biologically plausible implementation that facilitates learning and generalization in noisy and partially observable environments (Vértes and Sahani, 2019).

9.7 Multi-agent reinforcement learning

We have only considered the case of single agents interacting with a black-box environment. However, in many cases, multiple agents are simultaneously interacting with each other and the environment around them (Gronauer and Diepold, 2022). This means that, from the point of view of a single agent, the other agents are part of its environment. In such settings, there are interesting learning dynamics beyond the scope of the present tutorial, but which are covered in detail by e.g. Gronauer and Diepold (2022), and which are also of substantial interest in game theory (Nowé et al., 2012). In some cases, a whole group of agents may be working together to maximize a single joint reward function – as is the case for members of a single sports team. Interestingly, the learning of many individual neurons in the brain from a single common reinforcing

signal (such as dopamine) can be modelled as such a multi-agent reinforcement learning problem (Sutton and Barto, 2018). If the ‘agents’ (or neurons) are assumed to have Bernoulli-logistic outputs, Williams (1992) shows that the independent learning of individual agents from the global reward signal leads to the implementation of a policy gradient algorithm at the population level (Sutton and Barto, 2018).